

ISTANBUL TECHNICAL UNIVERSITY ★ GRADUATE SCHOOL OF SCIENCE
ENGINEERING AND TECHNOLOGY

**PREPARATION, CHARACTERIZATION AND IN VITRO EVALUATION OF
MULTIFUNCTIONAL MAGNETIC NANOPARTICLES FOR TARGETED
CANCER THERAPIES**

M.Sc. THESIS

Maide Gökçe BEKAROĞLU

Department of Science and Letters

Physics Engineering Programme

May 2015

ISTANBUL TECHNICAL UNIVERSITY ★ GRADUATE SCHOOL OF SCIENCE
ENGINEERING AND TECHNOLOGY

**PREPARATION, CHARACTERIZATION AND IN VITRO EVALUATION OF
MULTIFUNCTIONAL MAGNETIC NANOPARTICLES FOR TARGETED
CANCER THERAPIES**

M.Sc. THESIS

Maide Gökçe BEKAROĞLU
(509121109)

Department of Science and Letters

Physics Engineering Programme

Thesis Advisor: Assoc. Prof. Dr. Sevim İŞÇİ TURUTOĞLU

MAY 2015

İSTANBUL TEKNİK ÜNİVERSİTESİ ★ FEN BİLİMLERİ ENSTİTÜSÜ

**ÇOK FONKSİYONLU MANYETİK NANOPARÇACIKLARIN HEDEF
KANSER TEDAVİSİNDE KULLANILABİLMESİ İÇİN HAZIRLANMASI,
KARAKTERİZASYONU VE İN VİTRO ÇALIŞMALARI**

YÜKSEK LİSANS TEZİ

**Maide Gökçe BEKAROĞLU
(509121109)**

Fizik Mühendisliği Anabilim Dalı

Fizik Mühendisliği Programı

Tez Danışmanı: Doç. Dr. Sevim İŞÇİ TURUTOĞLU

MAYIS 2015

Maide Gökçe Bekaroğlu, a **M.Sc.** student of **ITU Graduate School of Science Engineering and Technology** student ID **509121109**, successfully defended the **thesis** entitled “**PREPARATION, CHARACTERIZATION AND IN VITRO EVALUATION OF MULTIFUNCTIONAL MAGNETIC NANOPARTICLES FOR TARGETED CANCER THERAPIES**”, which she prepared after fulfilling the requirements specified in the associated legislations, before the jury whose signatures are below.

Thesis Advisor : **Doc. Dr. Sevim İŞÇİ TURUTOĞLU**
İstanbul Technical University

Jury Members : **Prof. Dr. Yaşar Yılmaz**
İstanbul Technical University

Yrd. Doç. Dr. Ali Erçin Ersundu
Yıldız Technical University

Date of Submission : 4 May 2015
Date of Defense : 29 May 2015

To my family,

FOREWORD

This thesis was written for my Master degree in Physics Engineering at the İstanbul Technical University with help of fundings of TÜBİTAK. I would like to thank the following people, without whose help and support this thesis would not have been possible. First I like to show my gratitude to my thesis advisor Assoc. Prof. Sevim İşçi Turtoğlu for her kindness, suggestions, encouragements, valuable advices and support always when needed and guidance in writing the thesis and approaching the different challenges during the thesis. I want to thank Professor Fatma Neşe K  k for her support and advice for my research and for letting me use their lab equipment and facilities. I would like to thank all my proffesors for the knowledge they have given and for being great examples to look up to. Moreover, my colleague Yavuz i   i for all the help, support, friendship and the everlasting positive energy and motivation. Also to my colleague Eren Kargı for his friendship and moral support during this time. Finally I would like to thank my wonderful family , which I am very lucky to be a part of, for making me who I am today, espessially to my great parents and my little brother for their constant support during the hard times and the good times.

May 2015

Maide G  k  e BEKARO  LU
(Physics Engineer)

TABLE OF CONTENTS

	<u>Page</u>
FOREWORD.....	ix
TABLE OF CONTENTS	xi
ABBREVIATIONS	xiii
LIST OF TABLES	xv
LIST OF FIGURES	xvii
SUMMARY	xix
ÖZET	xxi
1. INTRODUCTION.....	1
2. MAGNETIC NANOPARTICLES	3
2.1. Magnetic Properties	3
2.1.1. Iron oxides.....	3
2.1.1.1 Size.....	4
2.1.1.2 Therapy with iron oxide nanoparticles.....	4
2.2. Multifunctional Core-Shell Nanoparticles	5
2.2.1. Multifunctional core-shell nanoparticle designs for therapy.....	6
3. COLLOIDS	9
3.1. Classification of Colloidal Systems	9
3.2. Colloidal Stabilization.....	10
4. RHEOLOGY AND ELECTROKINETIC PROPERTIES.....	13
4.1. Rheology	13
4.1.1. Flow models.....	13
4.2. Elektrokinetic Properties	16
4.2.1. Zeta potential.....	16
4.3. Magnetorheology	17
5. BIOPOLYMERS.....	19
5.1. Cellulose.....	19
5.2. Medical Applications of Biopolymers	20
6. EVALUATIONS OF TOXICITY (IN VITRO)	21
7. EXPERIMENTAL SECTION.....	23
7.1. Characterization of MNPs.....	23
7.2. Materials and Methods	24
7.3. Properties of Iron Oxide Particles.....	25
7.3.1. Rheological and electrokinetical properties.....	25
7.4. Synthesis of Biopolymer Coated Superparamagnetic Iron Oxide Nanoparticles	26
7.5. Interactions with HEC and Fe ₂ O ₃	27
7.5.1. Rheological properties	27
7.5.2. Electrokinetical measurements	28
7.5.3. Magnetorheology	29
7.5.4. Fourier transform infrared spectroscopy (FTIR)	31

7.5.5. X-Ray diffraction analysis (XRD)	32
7.5.6. Scanning electron microscope (SEM)	32
7.6. Interactions with NC and Fe ₂ O ₃	33
7.6.1. Rheological properties	33
7.6.2. Electrokinetical measurements	35
7.6.3. Magnetorheology	36
7.6.4. Fourier transform infrared spectroscopy (FTIR)	37
7.7. Drug Testing	38
7.7.1. Magnetic properties of synthesized Fe ₂ O ₃ nanoparticles	38
7.7.2. Thermo-gravimetric analysis (DT/TGA) of synthesized Fe ₂ O ₃ nanoparticles.....	39
7.7.3. In vitro evaluations	41
7.7.3.1 Mammalian cell culture	41
7.7.3.2 Cytotoxicity assays	41
7.7.4. Doxorubicin loading to Fe ₂ O ₃ nanoparticles	43
7.7.4.1 In vitro evaluations for DOX loaded nanoparticles	44
8. CONCLUSIONS	47
REFERENCES.....	51
CURRICULUM VITAE.....	55

ABBREVIATIONS

XRD	: X-ray diffraction
SEM	: Scanning electron microscope
FTIR	: Fourier transform infrared spectroscopy
IR	: Infrared
TG	: Thermo gravimetriy
DTA	: Differential thermal analysis
VSM	: Vibrating Sample Magnetometer
HEC	: 2-Hydroxyethyl cellulose
NC	: Nanocrystalline cellulose
Fe₂O₃	: Iron oxide
dH₂O	: Distilled water
MRD	: Magneto Rheolgical Device
TG-DTA	: Thermo gravimetric differential thermal analysis
hFOB	: Human osteoblast
MCF7	: Human breast adenocarcinoma
DMEM	: Dulbecco's modified Eagle's medium
FBS	: Fetal bovine serum
MTS	: [3-(4,5-dimethylthiazol-2-yl)-5-(3-carboxymethoxyphenyl)-2-(4-sulfophenyl)-2H-tetrazolium]
DOX	: (8s-cis)-10-[(3-amino-2,3,6-trideoxy- α -l-lyxo-hexopyranosyl)oxy]-7,8,9,10-tetrahydro-6,8,11-trihydroxy-8-(hydroxyacetyl)-1-methoxynaphthacene-5,12-dione hydrochloride
PBS	: Potassium phosphate buffer

LIST OF TABLES

	<u>Page</u>
Table 2.1 : Types of particles magnetic behaviour (Here spin magnetic moment is the magnetic moment induced by the spin of elementary particles).....	3
Table 2.2 : Characteristic Magnetic length scales for iron, maghaemite and magnetite.....	4
Table 3.1 : Classification of colloidal systems.....	9
Table 7.1 : Fe-O streching vibration peak values for different concentrations of HEC.....	32
Table 7.2 : Fe-O streching vibration peak values for different concentrations of NC.....	38

LIST OF FIGURES

	<u>Page</u>
Figure 2.1 : Therapy with MNPs: (a) by locating MNP +therapeutic molecules at the target organ with applied magnetic field. (b) by heating MNPs accumulated in the tumor using alternating magnetic field.....	5
Figure 2.2 : Magnetic nanoparticle carriers models.....	6
Figure 3.1 : Electric stabilization of colloidal dispersions.....	11
Figure 3.2 : Steric stabilization of colloidal dispersions	11
Figure 4.1 : Relation between applied force (to unit area) to velocity	13
Figure 4.2 : Flow Behaviour: (a) Shear stress- Shear rate. (b) viscosity - Shear rate graphs for Newtonian Fluids.....	14
Figure 4.3 : Shear stress- Shear rate graphs for Non-Newtonian Fluids	15
Figure 4.4 : Viscosity - Shear rate graphs for Non-Newtonian Fluids.....	15
Figure 4.5 : Simplified model of the electrical double layer. The Zeta potential is the electrical potential measured at the shear plane.....	16
Figure 5.1 : Chemical structure of cellulose.....	19
Figure 7.1 : Chemical structure representation of HEC	25
Figure 7.2 : Flow behavior: (a) Flow curves.(b) apparent viscosities of Fe ₂ O ₃ dispersions with different concentration.....	25
Figure 7.3 : Shear stress-shear rate graphs of: (a) all HEC concentrations with 2% Fe ₂ O ₃ dispersions. (b) 1g/L HEC+2% Fe ₂ O ₃ and 2% Fe ₂ O ₃ dispersions.....	27
Figure 7.4 : Apparent viscosity -HEC concentration graphs for all 2% Fe ₂ O ₃ dispersions with different HEC concentrations. Apparent viscosities were measured at different speeds (120, 200,250) of rheometer	28
Figure 7.5 : Zeta potential of 2% Fe ₂ O ₃ +HEC dispersions as a function of increasing HEC concentration	30
Figure 7.6 : Shear stress plotted as a function of shear rate: for suspensions containing different concentrations of HEC under test currents (a) 0A . (b)1A.	29
Figure 7.7 : FTIR spectrum of each sample of Fe ₂ O ₃ and Fe ₂ O ₃ in the presence of different HEC concentrations	31
Figure 7.8 : X-ray diffraction patterns of Fe ₂ O ₃ , 5x10 ⁻⁴ g/L HEC+ 2% Fe ₂ O ₃ and 1g/L HEC+ 2% Fe ₂ O ₃	32
Figure 7.9 : SEM images of 2% Fe ₂ O ₃ , 5x10 ⁻⁴ g/L HEC +2% Fe ₂ O ₃ and 1g/L HEC+ 2% Fe ₂ O ₃ respectively.....	33
Figure 7.10 : Shear stress-shear rate graphs of: (a) all NC concentrations with 2% Fe ₂ O ₃ dispersions. (b) 1g/L NC+2% Fe ₂ O ₃ and 2% Fe ₂ O ₃ dispersions.....	34

Figure 7.11 : Apparent viscosity-NC concentration graphs for all 2% Fe ₂ O ₃ dispersions with different NC concentrations. Apparent viscosities were measured at different speeds (120, 200,250) of rheometer	34
Figure 7.12 : Zeta potential of 2% Fe ₂ O ₃ + NC dispersions as a function of increasing NC concentration	35
Figure 7.13 : Shear stress plotted as a function of shear rate for suspensions containing different concentrations of NC under test currents (a)0A . (b)1A	36
Figure 7.14 : FTIR spectrum of each sample of Fe ₂ O ₃ and Fe ₂ O ₃ in the presence of different HEC concentrations	37
Figure 7.15 : Magnetization graphs for Fe ₂ O ₃ , 1g/L HEC+2% Fe ₂ O ₃ , 1g/L NC+2% Fe ₂ O ₃	39
Figure 7.16 : DT/TGA thermal analysis graph for 1g/L NC+2% Fe ₂ O ₃ , 1g/L HEC+ 2% Fe ₂ O ₃ , and 2% Fe ₂ O ₃	40
Figure 7.17 : Relative cell viability (%) of hFOB treated with 1g/L HEC + 2% Fe ₂ O ₃ , for 1g/L NC+2% Fe ₂ O ₃ and 2% Fe ₂ O ₃ (without biopolymer treatment) dilutions (25-400µg/ml) related to control wells	42
Figure 7.18 : Chemical structure representation of DOX	43
Figure 7.19 : Drug loading % of 1g/L HEC+2% Fe ₂ O ₃ , for 1g/L NC+2% Fe ₂ O ₃ particles	44
Figure 7.20 : Relative cell viability (%) of MCF-7 treated with DOX loaded 1g/L HEC+2% Fe ₂ O ₃ and 1g/L NC+2% Fe ₂ O ₃ particles.....	45

PREPARATION, CHARACTERIZATION AND IN VITRO EVALUATION OF MULTIFUNCTIONAL MAGNETIC NANOPARTICLES FOR TARGETED CANCER THERAPIES

SUMMARY

According to World Health Organization's statistics, it is expected that annual cancer cases will rise from 14 million in 2012 to 22 within the next 2 decades. Most common clinically used cancer treatments are surgery, chemotherapy, radiation therapy etc. However, these treatment options can be invasive and have many side effects. The major disadvantage of most chemotherapeutic approaches for cancer treatment is that they are non-specific for tumor tissue, hence toxicity to healthy cells and manifestation of side effects. To overcome these disadvantages, a new approach of using multifunctional magnetic nanoparticles (MNP) can eliminate the disadvantages of traditional treatments.

Popularly researched MNPs are iron oxides such as magnetite, maghemite, hematite and goethite for designing a multifunctional magnetic nanoparticle that can deliver drug to the target site. Recently, iron oxide nanoparticles (IONPs) have shown great potential in therapeutic and diagnostic applications, such as imaging, magnetic hyperthermia treatments and drug delivery systems. IONPs, biocompatibility in moderate doses, easy of surface modification, known metabolic pathways, variety of their sizes and their magnetic properties allow them to be suitable for therapeutic applications. These properties and their ability to be manipulated upon application of a magnetic field allow them to be utilized as therapeutic and diagnostic tools. Iron oxide nanoparticles have been widely used in preclinical experiments for imaging, magnetic hyperthermia and drug delivery.

Besides the advantages mentioned above, IONPs also might cause cytotoxicity and can form free radicals in the system. For this reason, these particles must be modified to reduce these effects. One of the most sensitive parameters in toxicity is the surface coating of the nanoparticles. To induce lower toxicity, nanoparticles can be coated with biocompatible coating, which is an easier, cheaper method comparing to synthetic polymers. Also loading anti tumor drugs to MNPs surface is challenging without the help of an polymer. so using biocompatible biopolymers for the functionalization of nanoparticles by modulating physical and chemical properties (surface charge, etc.) improving stability, reducing toxicity and protection of drugs and nanoparticles may eliminate existing disadvantages. Also evaluating the toxicological effects of MNPs both *in vitro* and *in vivo* is crucial for the development of MNPs. Therefore, this research reports the synthesis, characterization, and *in vitro* evaluations of multifunctional magnetic iron oxide nanoparticles coated with biopolymers. This reported nanodrug system could potentially open up new possibilities in the design of therapeutic agents using multifunctional nanoparticles.

When designing and synthesizing multifunctional nanoparticles all advantages and disadvantages previously mentioned must be considered. To reach a positive result characterization, optimum polymer concentration determination is important. Optimum concentration of the biopolymers can be determined by characterization of the colloidal properties of the MNP particles. The desired MNP-biopolymer structure suitable for targeted drug delivery must have fully covered surfaces by the biopolymers and stable structures. The flocculation properties of MNPs can be determined by their rheological measurements and the surface properties can be determined by their electrokinetical measurements. The hydrodynamic radius of the MNPs can be controlled by the light scattering experiments. Characterization provides an opportunity to analyze the results of experiments and to choose the next step to achieve expected results. Characterization techniques are required to determine magnetic nanoparticle properties such as size, crystal structure, material's thermal stability, absorption spectrum and magnetic behavior. Characterization of nanostructured materials is important because human eye cannot determine such small structures and their properties. The stable and fully covered surfaces of the MNPs were characterized by the conventional methods such as scanning electron microscope (SEM) for the determination of the size and morphology, X-ray diffraction (XRD) to determine crystal structure, Fourier transform infrared spectroscopy (FTIR) to analyze the chemical bonds and functional groups, thermogravimetric analysis (TGA) to determine material's thermal stability and vibrating sample magnetometers (VSM) to measure the magnetic properties. After the characterization of MNP, the *in vitro* evaluations will give insight about biological compatibility and toxicity of synthesized particles.

The only possibility of the targeted drug delivery of magnetic particles is to apply external magnetic field. However, when an external magnetic field is applied there is a drastic change on the flow properties of the magnetic suspensions. The magnetorheological effect of the drug delivery MNPs are rarely researched in the literature and very important considering the applications. In this study we examined MNPs magnetorheological properties.

The main purposes this project is to have stable and fully covered surfaces of Fe_2O_3 particles by coating with HEC and cellulosic polymers and to obtain non-toxic biocompatible multifunctional magnetic particles. When particles reach desired properties cancer drugs will be adsorbed on the particles and the effect of these particles on the cancer cells will be examined.

To achieve the goals mentioned above Fe_2O_3 particles were treated with biopolymers in a variable range of polymer concentration. Particles with optimum polymer concentrations were characterized and tested for toxicity. The reported nanodrug system in this thesis showed that multifunctional nanoparticles synthesized could potentially open up new possibilities in the design of therapeutic agents using them. Future efforts could be to investigate the *in vivo* characteristics of these integrated nanostructures.

ÇOK FONKSİYONLU MANYETİK NANOPARÇACIKLARIN HEDEF KANSER TEDAVİSİNDE KULLANILABİLMESİ İÇİN HAZIRLANMASI, KARAKTERİZASYONU VE İN VİTRO ÇALIŞMALARI

ÖZET

Nanoteknoloji son zamanlarda ilaç endüstrisinde, teşhis ve tedavilerde, görüntüleme tekniklerinde, vücutta kontrollü ilaç salınımı ve ulaştırmada, doku mühendisliğinde, vs. kullanılmaya başlanılmıştır. Birçok farklı nanosistemlerden özellikle çok fonksiyonlu manyetik nanoparçacıklar (MNP) bu konuda çok ilgi çekmektedir. MNPlerin manyetik alan altında yönlendirilebilmesi özelliği diğer nanoparçacık sistemlerine göre daha avantajlı parçacıklar olmalarını sağlamaktadır. Yeni nesil tedavi yöntemlerinde sağlıklı hücrelere zarar vermeden ilaç ulaştırma, hedef kitleye tedavi için özellikle MNP kullanımları ve avantajları araştırılmaktadır.

Dünya Sağlık örgütünün yayımladığı istatistiklere göre önümüzdeki 20 yılda görülen kanser vakalarının 22 milyon gibi bir sayıya ulaşması beklenmektedir. Çok yaygın olarak görülen ve ölüm oranları yüksek olan bu hastalığın tedavi yöntemleri sadece kemoterapi, radyoterapi ve ameliyat ile sınırlıdır. Bu yöntemler yan etkisi çok olan ve invazif yöntemlerdir. Kanser tedavisi için en çok kullanılan yöntemlerden biri olan kemoterapi yönteminin en büyük dezavantajı spesifik olmaması ve tümör dokusu dışında sağlıklı hücrelere de zarar vermesidir. Bu yöntemlere alternatif olarak hedeflendirilmiş ilaçlar düşünülebilir. Bu parçacıklar lokalize halde istenilen bölgeye ulaştırılabileceği için geleneksel tedavi yöntemlerinde görülen yan etkileri azaltabilir. Hedeflendirilmiş ilaçlar, seçilmiş etki bölgesi veya bölgelerinde en uygun etkileşmeyi sağlayabilmektedir. Ayrıca, etken maddenin dozunun azaltılabilmesine ve etken maddenin sadece hedef bölgeye dağılımıyla sınırlandırılmasına olanak sağlayabilmektedirler. Böylece oluşabilecek herhangi bir yan etki veya yan etkiler büyük oranda minimuma indirilebilecektir.

Günümüzde, hedeflendirilmiş ilaç modeli için çok fonksiyonlu manyetik nanoparçacıkların (MNP) kullanılması araştırmacılar tarafından çok ilgi görmektedir. Bu parçacıklar gerekli modifikasyonlarla ilaç yüklenmeye uygun ve manyetik alan ile istenilen bölgeye ulaştırılabilen parçacıklar haline getirilebilirler. Bu yöntem ile geleneksel kemoterapinin aksine sadece tümörlü hücrelere müdahale edilebilir ve ilaçların sağlıklı hücreleri etkisi azaltılabilir.

MNP ile tümörlere üç farklı yol ile müdahale edilebilir. Bunlar: 1- hedef hücre tedavisi için MNP'lere ilaç yüklemesi, 2- tümörü MNP ile yüksek sıcaklıklara (dış manyetik alan etkisi ile) çıkararak yakmak, 3- spesifik biyomolekülleri MNP'lere bağlayarak tümörlere müdahale etmektir. Hedef hücrelere anti-tümör ajanları ulaştırarak tedavi etmek geleneksel kemoterapi yöntemine karşılık umut verici, alternatif bir yöntemdir. MNP olarak genelde demiroksitler, demir, kobalt gibi parçacıklar kullanılır.

MNPler biyoyumlu olduğu düşünülse bile, vücuda alındığında toksik etki ve serbest radikal oluşumu gösterebilmektedir. Bu parçacıkların toksik etkisine sebep olan

başlıca nedenlerden biri parçacıkların yüzey yükleridir. Ayrıca farklı bir dezavantaj ise MNPlerin kolloidal özelliklerinden dolayı stabil hale getirilmedilerse, bir araya toplanıp çökme eğilimleri olmasıdır. Bu dezavantaj parçacıkların vücut içine alındığında kan dolaşımına giremelerini engellemektedir ve çeşitli yan etkilere sebep olabilmektedir. Amaca uygun bir yapıda hedeflendirilmiş ilaç tasarımı yapabilmek için tasarım aşamasında yukarıda belirtilen tüm dezavantajlar göz önüne alınmalıdır.

Çökme davranışını ve toksik etkilerini iyileştirmek biyopolimerler ile mümkündür. Bu etkilerin elimine edilmesi için yüzeylerinin biyolojik uyumlu hale getirilmesi gerekmektedir. Bu amaçla MNP yüzeyleri biyopolimerler, grafen gibi malzemeler ile kaplanabilirler. Bu polimerler biyo uyumlu ve biyo çözünür oldukları için ilaç modellerinde kullanımı sentetik polimerlere göre daha avantajlıdır. Biyopolimerler ile kaplama diğer tekniklere göre daha ucuz ve kolay erişilebilir bir yöntemdir ayrıca biyopolimerler anti tümör ilaç yüklemeleri ve parçacıkları stabil hale getirilmeleri için iyi bir altyapı sağlamaktadır. Toksik etkileri azaltmak için kullanılacak her bir MNP'nin tüm yüzeyinin biyopolimer ile kaplanması gerekmektedir.

MNP'lerin kolloidal özellikleri belirlenerek kararlı parçacıklar elde etmek için gerekli biyopolimer konsantrasyonları seçilebilir. Burada istenilen MNP yüzeylerinin biyopolimerler ile tamamen kaplı ve kararlı yapılar olmasıdır. Reolojik ölçümler ile dispersiyonların akış özellikleri ve floküle olup olmadığı, magnetoreolojik ölçümlerle manyetik alan altındaki akış özellikleri, elektrokinetik ölçümler ile yüzeylerin kaplanıp kaplanmadığını, ışık saçılması deneyleri ile hidrodinamik yarıçaplarını, parçacık boyutlarını ve tüm bu yöntemlerin birlikte yorumlanması ile sistemin kararlı olup olmadığını belirleyebiliriz. Kararlı, yüzeyleri tamamen kaplı demir oksitlerin geleneksel karakterizasyonları ile görüntüleyebilir (Taramalı elektron mikroskopu (SEM), X-ışınları difraksiyonu (XRD), fourier transform infrared (FTIR) gibi yöntemler ve kolloidal karakterizasyon sonuçları desteklenebilir. Bunlar ile birlikte biyodemirlerin manyetik ve termal karakterizasyonları da önemli bilgiler taşırlar. Titreşimli numune magnetometresi (VSM), termal testleri (DSC, TGA) gibi testlerin yapılması biyopolimer kaplı demir oksitlerin manyetşk ve termal davranışlarını belirlemek için önemlidir. Karakterizasyonların ardından biyodemirlerin gerçekten canlı hücrelere zarar verip vermediği canlı dışı (in-vitro) hücre deneyleri ile kontrol edilebilir ve ilaç yüklemesi yapıldıktan sonra kanser hücrelerine etkisi gözlemlenebilir.

Tez çalışmasındaki amaçlar; MNP olarak kullanacağımız demiroksit (Fe_2O_3) parçacıklarının üzerine literatürde henüz çalışılmamış olan hidroksietil selüloz (HEK) polimerini ve nanokristal yapıdaki ağaç fiberlerinden elde edilen selülozik polimeri (NK) kullanarak MNP parçacıklarının kolloidal özelliklerini takip ederek kararlı ve MNP parçacıklarının yüzeylerini tamamen kaplanmış numuneler elde etmek, polimerlere antitümör ajanları adsorbe ettirerek antikanser özellikli ve manyetik alan ile yönlendirilebilen nanoparçacıklar elde etmek ve hedeflendirilmiş ilaç literatürüne katkıda bulunmak, son olarak çağımızın hastalığı olan kanserin tedavisine yönelik çalışmalara katkıda bulunmak, literatürde kullanılmayan HEK ve selülozik polimerlerin kullanılması ile literatüre katkıda bulunmaktır.

Belirtilen amaçlara ulaşmak için yapılması gerekenler; Sistemlerin akış özellikleri, zeta potansiyelleri ve parçacık boyutları bilgisi ile polimer konsantrasyonuna bağlı değişimlerini ve etkileşimlerini belirlemek, numunelerin yukarıda belirtilen geleneksel karakterizasyonları yapmak ve kolloidal karakterizasyon sonuçları ile

uyumu arařtırmak, biyopolimer kaplı demiroksitlerin sitotoksitesini canlı dıřı (in-vitro) hücre deneyleri ile arařtırmak, toksik etkiyi minimuma indirmek, *in vitro* deneyler ile saėlıklı hücreler ile etkileřimlerini belirleyerek kullandığımız biyopolimerlerin bu tip uygulamalar için uygunluėunu kontrol etmek ve son olarak biyopolimer kaplı demir oksitlere antitümör ajanlar yüklenerek ve yine in-vitro sitotoksitesini deneyleriyle kanserli hücreler üzerindeki etkisi arařtırmaktır. Bu basamakları uygulayarak belirtilen tüm deneyler yapılmıřtır ve sonuçları tezde açıklanmıřtır.

Deney sonuçlarına göre sentezlediğimiz çok fonksiyonlu manyetik nanoparçacıkların kanser tedavisi için kullanılabilecek hedeflendirilmiř ilaç olabilmeye uygun parçacıklar olduėu söylenebilir ve ileride yapılacak terepâtik ilaç tasarımlarıyla ilgili çalıřmalara yardımcı olacak bilgiler saėlayabilecegi söylenebilmektedir. Çalıřmalarımızın devamında sentezlediğimiz parçacıkların *in vivo* (canlı içi) testlerindeki davranıřlarını arařtırmak istemekteyiz.

1. INTRODUCTION

Over the last decade, nanotechnology has been applied in many industrial sectors, including medicine. New generation of targeted drug delivery systems for cancer therapy with nanoparticles are highly researched recently. The major disadvantage of most chemotherapeutic approaches for cancer treatment is that they are non-specific for tumor tissue, hence toxicity to healthy cells and manifestation of side effects. To overcome these disadvantages, multifunctional magnetic nanoparticles (MNP) can be used. The targeted delivery of anti-tumor agents adsorbed on the surface of MNP's is a promising alternative to conventional chemotherapy. MNPs can be located at the targeted site with external magnetic fields and release the drugs adsorbed to their surfaces. Magnetic nanoparticles, although may contain other elements, are often iron oxides. Most commonly used MNPs are, iron oxides such as magnetite, maghemite, hematite and goethite.

Especially iron oxide nanoparticles (IONPs) attract great attention in biomedical applications due to their biocompatibility in moderate doses, easy surface modification properties, their relatively well known iron metabolic pathways, variety of their sizes and shapes and their magnetic properties. These properties and their ability to be manipulated upon application of a magnetic field allow them to be utilized as therapeutic and diagnostic tools. Iron oxide nanoparticles have been widely used in preclinical experiments for imaging, magnetic hyperthermia and drug delivery. In order to successfully transform these applications to clinical trials their physicochemical, toxic and functionalization properties must be improved.

Because of the physiological relevance of iron, MNPs were initially considered to be non-cytotoxic. However, it has been shown that due to the small sizes of MNPs can reach high local concentrations within the cells and might cause cytotoxicity. Furthermore, free iron can form free radicals, which can be harmful to neural tissues [1]. For this reason, these particles must be modified to reduce these effects. One of the most sensitive parameters in toxicity is the surface coating of the nanoparticles.

The negatively charged uncoated MNPs have been shown to exhibit cytotoxicity above a certain threshold amount. Uncoated MNPs also have low solubilities and they are less stable which results in nanoparticle precipitation in aqueous media. In order to reduce the toxicity of MNPs, different coatings have been used. Such as polymers or biopolymers. Coated nanoparticles induce lower toxicity due to the presence of the biocompatible coating and the lower adsorption sites for proteins, ions and other components in the cell medium [2,3]. Nanoparticles coated with biocompatible coating could induce lower toxicity. Also loading anti tumor drugs to MNPs surface is challenging without the help of a polymer. Biocompatible biopolymers have provided a strategy for the functionalization of nanoparticles by modulating physical and chemical properties (surface charge, etc.) improving stability, and protection of drugs and nanoparticles [4, 5].

The main purpose of this thesis is to have stable and fully covered surfaces of iron and iron oxide (Fe_2O_3) nanoparticles by controlling the colloidal properties with cellulosic polymers. The interactions of the polymer and iron oxide (Fe_2O_3) nanoparticles can define the flow properties of the system, the zeta potential values, and the magnetorheology. In order to reach previously mentioned goals colloidal characterizations will be performed. The conventional characterization of the samples will also be performed to compare the colloidal characterization results. The *in vitro* evaluations will be performed to see that whether there are any changes on the toxicity or not. The anti-tumor drugs will be adsorbed on the Fe_2O_3 -biopolymer structures and the effect of them on cancer cells and their drug loading efficiencies will be controlled. In this study, biopolymer coated iron oxide nanoparticles were synthesized, by following the steps mentioned above, to obtain a multifunctional core shell nanostructure, which can be used for targeted drug delivery systems for cancer therapy [6-9].

2. MAGNETIC NANOPARTICLES

The magnetic properties, electronic properties and reduced sizes of magnetic nanoparticles (MNP) provide many advantageous characteristic properties to the nanoparticles. Magnetic properties of MNP's depend on their size, shape, structure, crystallinity, synthesis method and chemistry. Most popular MNP's used for many kinds of applications are iron, cobalt and nickel compounds [10-12].

2.1 Magnetic Properties

Magnetic dipole moments of an unmagnetized material are randomly orientated. When a material is placed in a magnetic field these moments tend to align themselves in relation to magnetic fields direction. By the materials reaction to a magnetic field, all substances are categorised into several groups as, diamagnetic, paramagnetic, ferromagnetic and superparamagnetic materials.

Diamagnetic materials create a magnetization opposite to the direction of applied magnetic field. Paramagnetic materials that are attracted by an externally applied magnetic fields and they form a magnetization in the direction of applied magnetic field. And ferromagnetic materials such as iron form permanent magnets, or are attracted to magnets after undergoing certain mechanisms (like temperature change) [13-16]. The basic types of magnetic behaviour examples are explained in Table 2.1.

Table 2.1: Types of particles magnetic behaviour (Here spin magnetic moment is the magnetic moment induced by the spin of elementary particles).

Type	Spin Alignment
Ferromagnetic	All spins align parallel to one another; spontaneous magnetization
Paramagnetic	Spins tend to align parallel to external magnetic field
Diamagnetic	Spins tend to align antiparallel to external magnetic field

2.1.1 Iron oxides

Most popular nanoparticles used for magnetic core structures are iron oxides: magnetite (Fe_3O_4) and maghemite ($\gamma\text{-Fe}_2\text{O}_3$). Both magnetite and maghemite have cubic spinel structures. Magnetite (IUPAC name: (II, III) oxide) is a black or grayish

material which contains divalent and trivalent Fe ions and has a chemical formula of Fe_3O_4 or $\text{FeO} \cdot \text{Fe}_2\text{O}_3$. For magnetite, net magnetization occurs due to Fe^{2+} ions from octahedral sublattice. Magnetite is sensitive to oxidation and can oxidize its Fe^{2+} ions and transform into maghemite. Maghemite is formed by oxidation of magnetite. Contains only trivalent Fe ions and its International Union of Pure and Applied Chemistry (IUPAC) name is iron (III) oxide. Chemical formula of Maghemite is $\gamma\text{-Fe}_2\text{O}_3$ and has a brownish color. Crystal structure is similar to magnetite, but with vacancies in octahedral sites due to oxidation [17, 18].

2.1.1.1 Size

Size of the nanoparticle is important for determining properties of the system; this is arguably the most important parameter upon which any IONPs system must be designed. Size of the particles affect the dynamics of the magnetic moments in magnetic NPs, also particle size is important in the detection and internalization IONPs inside mammals. Magnetic scale lengths such as superparamagnetic radius (R_{SPM}) and the single domain radius (R_{SD}) characterize magnetic NP systems. R_{SPM} is the maximum particle size up to which a superparamagnetic regime is observed and R_{SD} indicates the value below which the formation of magnetic domains is no longer energetically favourable [19]. Table 2.2 summarizes these parameters for maghemite and magnetite, the most commonly used iron oxides in biomedicine.

Table 2.2: Characteristic magnetic length scales for iron, maghemite and magnetite [20-22].

	R_{SD} (nm)	R_{SPM} (nm)
Maghemite	42.5	17.5
Magnetite	52.7	12.2
Iron	8.3	8.0

2.1.1.2 Therapy with iron oxide nanoparticles

In the last few years, IONPs have also been demonstrated to be useful in clinical settings. Mostly researched areas of therapy with MNPs are targeted delivery and thermotherapy. Many targeting agents like MNPs, liposomes, micelles dendrimers, artificial DNA nanostructures etc, can perform targeted delivery. Iron oxide NPs have been successfully used as a carrier for bioactive molecules in a number of conditions both *in vitro* and in animal models [23, 24].

Another promising application of MNPs is thermotherapy of solid tumours. The principle of hyperthermia therapy involves the administration of an IONPs fluid within the tumour, followed by the application of an alternating magnetic field which increases temperature of the targeted region up to 41-46 °C. The temperature increase causes cellular hyperthermia, which induces apoptosis. Clinical studies for the application of thermotherapy showed promising results for many studies. Using IONPs in humans were initiated in 2007 on prostate cancer and glioblastoma patients. Afterwards, different clinical assay were carried out for prostate cancer metastatic bone cancer recurrent glioblastoma etc. showed tumor necroses with well-tolerated results and minor or no side effects [25-31]. The illustration of MNP therapy mechanism examples can be seen in Figure 2.1.

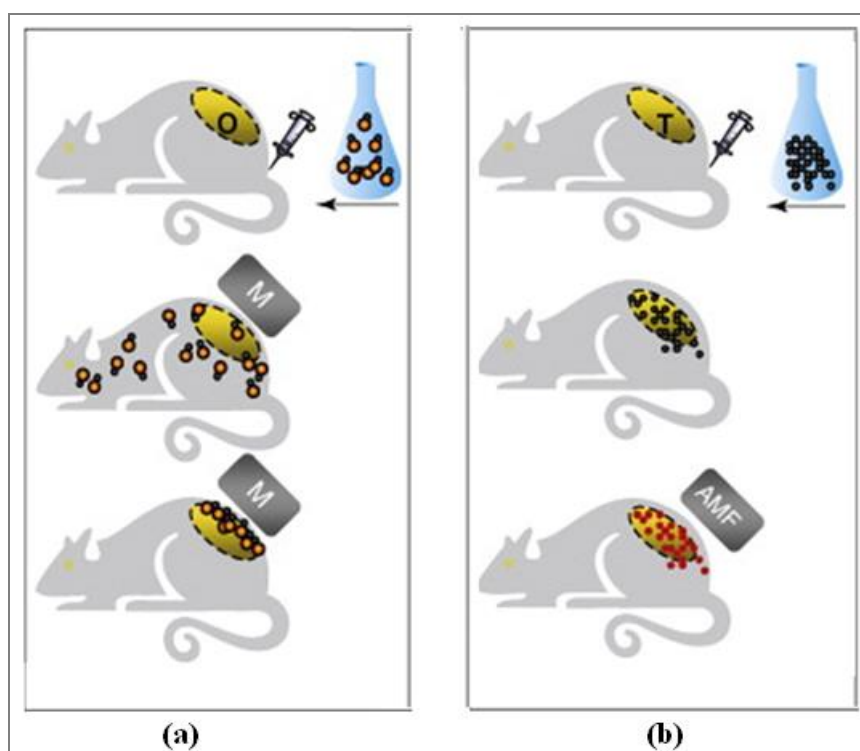


Figure 2.1 : Therapy with MNPs: (a) by locating MNP +therapeutic molecules at the target organ with applied magnetic field. (b) by heating MNPs accumulated in the tumor using alternating magnetic field [32,33].

2.2 Multifunctional Core-Shell Nanoparticles

As mentioned above magnetic nanoparticles have many advantageous properties like manipulation by an external magnetic field and their reduced sizes. These properties could be beneficial for many applications from various fields such as medicine, biomedical, diagnostic (MRI contrast agents), theurapathic (drug delivery), etc.

Magnetic carrier nanoparticles can allow transportation to a desired location through the control of a magnetic field [33]. Surface coating and functionalization of MNP's may be required to ensure stability, improve biocompatibility and reduce toxicity to achieve most efficient results.

2.2.1 Multifunctional core-shell nanoparticle designs for therapy

Magnetic nanoparticle carriers consist of three functional parts: a magnetic core, a surface coating, and a functionalized outer coating (Figure 2.2). At the center of the carrier is the superparamagnetic core which allows for the magnetic manipulation of the particle in the presence of an external magnetic field. The composition of the magnetic core is dependent on the application. For example, magnetite (Fe_3O_4) and maghemite ($\gamma\text{-Fe}_2\text{O}_3$) with high oxidative stability are currently the only accepted nontoxic magnetic materials for medical applications [34-36].

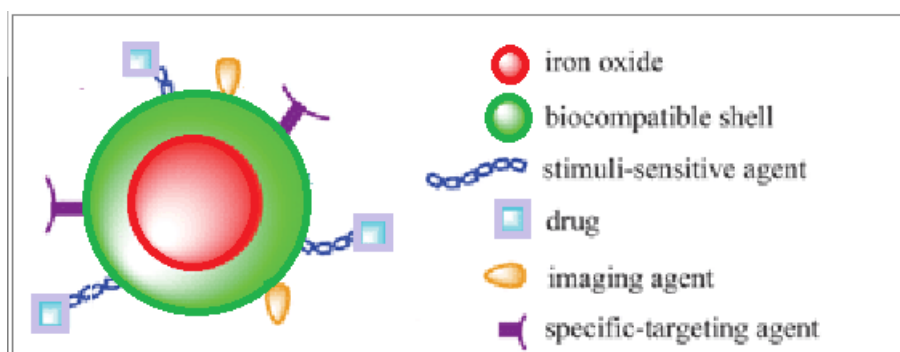


Figure 2.2 Magnetic nanoparticle carrier models.

There are many researchs done about multifunctional core-shell nanoparticle for medical applications such as drug delivery, targeting, imaging, etc. One of the main promising therapeutic applications of coated magnetic nanoparticles is for targeted chemotherapeutic drug delivery to tumors. Because of their magnetic manipulation properties nanoparticles coated with a drug could be injected intravenously, transported to a target site (e.g., cancerous tumor) and be retained at the site by application of a magnetic field. This form of drug design can increase specificity of the drug, localized drug levels significantly, hence doses required for systemic drug delivery and potential toxic side effects at nontargeted tissues can be reduced [33-37].

Another interesting technique is using of implanted magnetized stents which can capture magnetic particles carrying desired drugs. This technique can allow

reapplication without elimination, and localization of the drugs at optimum doses. A second important therapeutic application is in the field of hyperthermia, which involves heating organs or tissues to between 41 and 46 °C to obtain tumor cell necrosis. The application of an external alternating magnetic field to nanosized magnetic particles causes heating via hysteresis energy losses [37-41].

3. COLLOIDS

The term colloid was first used in 1861 by Thomas Graham for the suspensions of liquid or solid phases in another liquid. Currently the term colloid is used for dispersed insoluble particles suspended throughout another liquid substance [41,42].

Particle size is one of the most important parameter that determines the properties of colloidal systems. Colloidal particles have a size range of 10^{-3} to 1 mm. Recently very small nano sized colloidal particles attract great attention for studies [41].

Colloids usually have electrical charges. Main contributions to surface charges of colloids are due to isomorphic substitutions, chemical reactions and absorbing ions. Colloids can that remain dispersed in a liquid for a long time due to their small size and electrical charge so it can be said that electrical charges affect colloidal behaviour and dispersion properties. Double layer forces occurring between charged objects across liquids can affect the systems rheological properties and its zeta potential [42, 43].

3.1 Classification of Colloidal Systems

Classification of colloidal systems can be done according to colloidal particle size or according to the phase (solid, liquid, or gas) of the dispersed substance and of the medium of dispersion. Generally, the latter classification is used for colloidal systems and some examples of this classification system are given in Table 3.1.

Table 3.1: Classification of colloidal systems [41, 42].

Kolon A	Kolon B	Kolon C
Solid	Gas	Aerosol
Liquid	Gas	Aerosol
Solid	Liquid	Sol or Colloidal Sol
Liquid	Liquid	Emulsion
Gas	Liquid	Foam
Solid	Solid	Solid Sol
Liquid	Solid	Solid Emulsion
Gas	Solid	Solid Foam

The interaction forces acting between colloidal dispersions play an important part in determining the properties of the dispersion. These forces occur when double layer systems or particles interact in the dispersion.

Brownian motion is an irregular motion exhibited by particles of matter when suspended in a fluid. Brownian motion, being independent of all external factors, is dependent to the thermal motion of the particles in the dispersion. This movement behaviour is observed for all types of colloidal suspensions but force types can differ to be attractive or repulsive depending on the structure of the system. The interaction distances between colloidal objects can affect the forces acting. Main reason for repulsive forces is van der Waals forces [41- 45].

The Derjaguin–Landau–Verwey–Overbeek (DLVO) theory is built on the assumption that the forces between surfaces in a dispersion can be regarded as the sum of the contributions of the forces below.

- Brownian motion and diffusion
- Electrical double layer forces
- van der Waals forces
- Born forces

3.2 Colloidal Stabilization

Small particles in the dispersion can move freely in colloidal systems. Brownian motion of these small colloidal particles leads to an increased chance of collisions in the dispersion. For some systems particles do not separate after the collision (exp. salt or polymer added systems) and collisions continue to happen more particles are stuck to each other causing decreased mobility to particles in the dispersion. These events can lead to aggregation or phase separation. Because dispersed particles tend to reduce the large interfacial area by aggregation or phase separation to a continuous phase. Gathering of particles in a dispersion is called flocculation when polymer is present. Stabilization is required to prevent flocculation of particles for colloidal dispersions. Two mechanisms are known for stabilizing the colloidal state are, electric stabilization and steric stabilization (Figure 3.1 and Figure 3.2) [46, 47].

Electric stabilization occurs when the electric charges of the particles are same. repulsive forces between the particles stabilizes the system. Steric stabilization

overcomes flocculation by adsorption of nonionic surfactants or polymers onto particle surface. The second method is the most effective method for overcoming flocculation and stabilization. A combination of the two mechanisms is also possible for some colloidal systems where aggregation mechanism is inhibited by both electrostatic and steric stabilization. This kind of stabilization is called electrosteric stabilization and it is usually associated with the adsorption of polyelectrolytes onto the particle surface [47, 48].

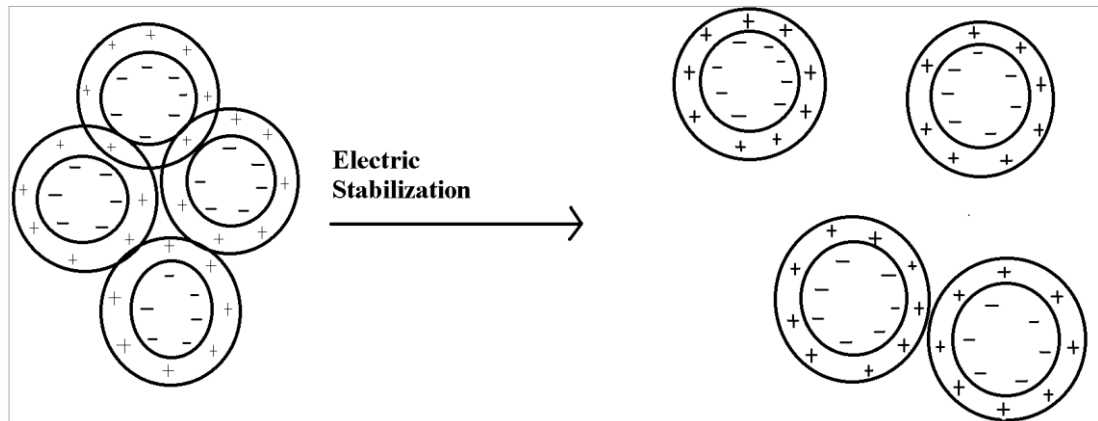


Figure 3.1: Electric stabilization of colloidal dispersions.

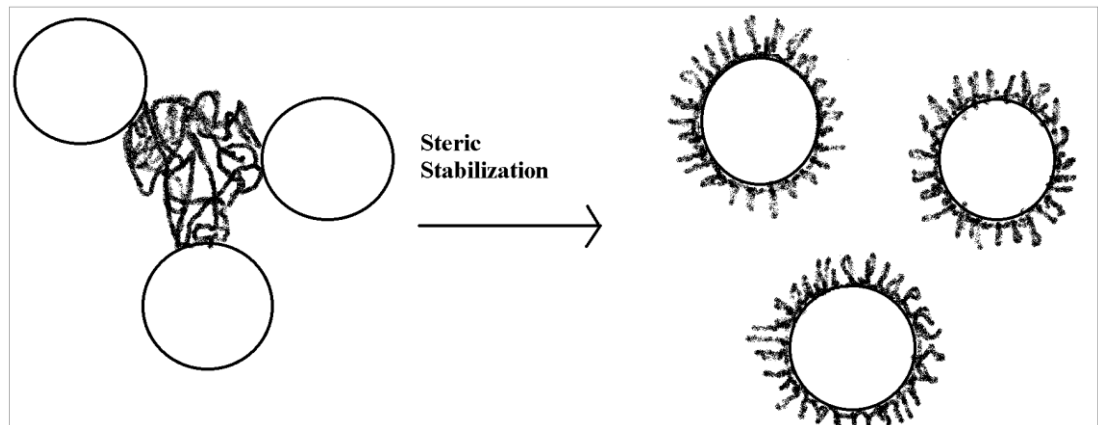


Figure 3.2: Steric stabilization of colloidal dispersions.

4. RHEOLOGY AND ELECTROKINETIC PROPERTIES

4.1 Rheology

The interactions between particles in a disperse system determine the flow characteristics (rheology) of these systems. The term 'Rheology' was first used by Professor Bingham as a definition of the study of deformation and flow of the matter. All fluid flow properties are called 'rheological properties'. Establishing the relationship between applied forces and geometrical effects induced by these forces at a point in a fluid is one of the purposes of rheology. Some of the subjects of rheology are elasticity, plasticity and viscosity [48, 49].

4.1.1 Flow models

Flow behaviour of fluids is determined according to movement of fluid boundary layers. According to Newton's model when a force F is applied to first layer of two boundary layers with a surface area of A (apart with a distance of dy), while the second layer is stationary, the velocity of the first layer will increase by an amount of dv (Figure 4.1). Here dv/dy is determined as shear rate or shear gradient and its unit is s^{-1} . F/A is determined as shear stress and its unit is Pascal (Pa) [48-53].

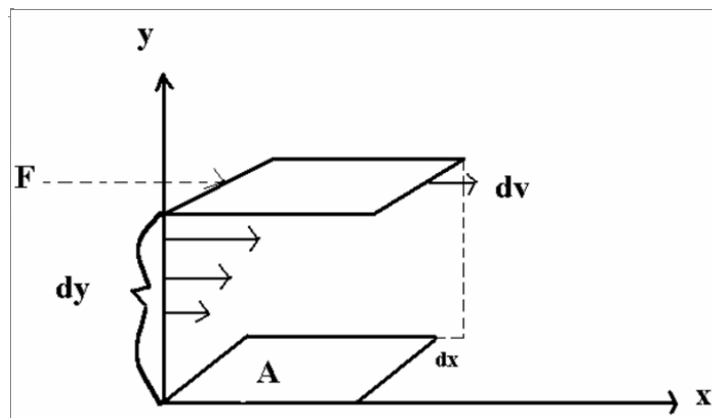


Figure 4.1: Relation between applied force (to unit area) to velocity.

When the shear stress between the layers of a fluid is directly proportional to the shear rate, the fluid is determined as a Newtonian fluid. The viscosity is independent of shear rate for Newtonian fluids (Figure 4.2). To determine the flow behaviour of a Newtonian fluid, viscosity measurements will be enough. The mathematical representation is given below for Newtonian Fluids.

$$\text{Shear stress: } \tau = F/A, \quad (4.1)$$

$$\text{Shear rate: } \gamma = dv/dy \quad (4.2)$$

$$F/A = \eta \cdot dv/dy \quad (4.3)$$

$$\tau = \eta \cdot \gamma \quad (4.4)$$

All fluid flow behaviours can be determined by plotting their Shear rate- Shear stress graph.

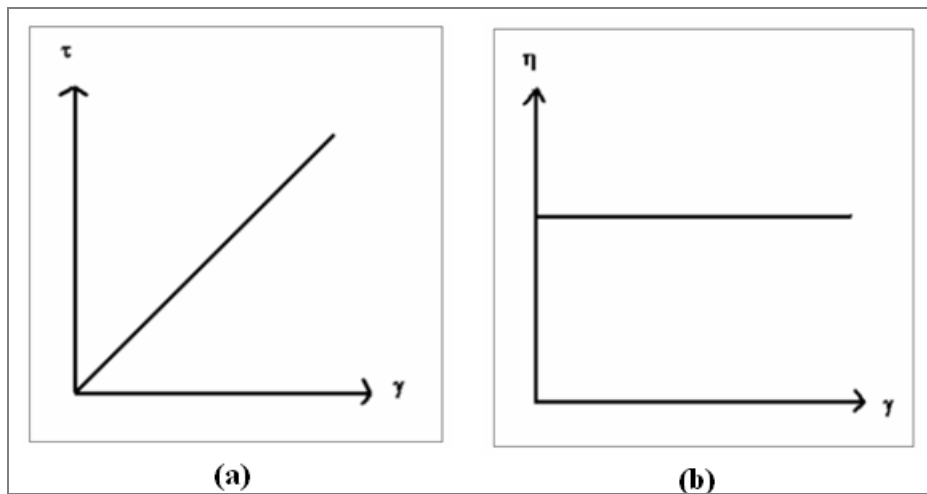


Figure 4.2: Flow Behaviour: (a) Shear stress- Shear rate. (b) viscosity - Shear rate graphs for Newtonian Fluids

Any fluid that does not obey Newton's law of viscosity is a non-Newtonian fluid. For non-Newtonian fluids, linearity is distorted as particles interact with each other and lose energy. Constant that determines viscosity alters as shear rate or shear stress changes. Because of these characteristics of flow behaviours two kinds of viscosity is determined to explain flow of non-Newtonian fluids and these are; plastic and apparent viscosities. Apparent viscosity is a measure of the resistance of a fluid, which is being deformed by either shear stress or applied forces. Plastic viscosity is

the slope of the shear stress/shear rate line above the yield point where flow is linear between certain shear rate values [48-53].

Fluid flow behaviours can be determined by plotting their Shear rate- Shear stress graphs. Non-Newtonian fluids are grouped as plastic, Bingham plastic, shear thinning (pseudoplastic), shear thickening (dilatant) fluids. Many constitutive models are available in the literature that describes the rheology of purely viscous fluids [48-53]. Basic Non-Newtonian fluid flow behaviours can be seen in Figure 4.3 and Figure 4.4.

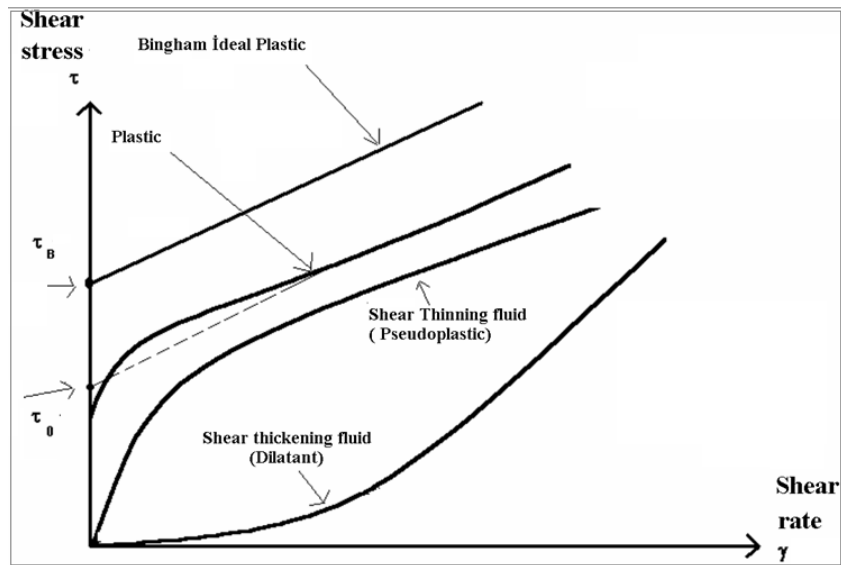


Figure 4.3: Shear stress- Shear rate graphs for Non-Newtonian Fluids.

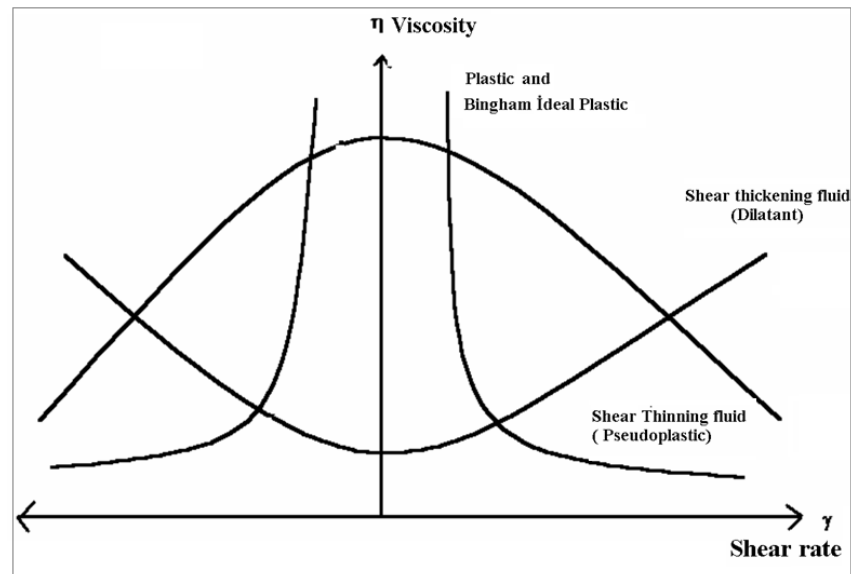


Figure 4.4: Viscosity - Shear rate graphs for Non-Newtonian Fluids.

4.2 Elektrokinetic Properties

4.2.1 Zeta potential

Particle interactions and stability of dispersion can be affected by electrokinetic effects. Zeta potential (ζ) is the measurement of these electrokinetic effects. The electrical double layer consists of two layers of ions from solution, which neutralize the surface charge, as shown in Figure 4.5. Colloidal particles like iron oxide nanoparticles are charged on the surface when dispersed in a solvent. Charged surfaces of the particles attract opposite charge ions to their surfaces. The electrical double layer consists of two layers of ions from solution, which neutralize the surface charge, as shown in Figure 4.5. The surface on the particle is immobile and it is called the Stern layer. The diffuse layer is much thicker, and is a layer that is enriched with ions with opposite charge as the surface. In addition, the near boundary between the Stern layer and the diffuse layer is the shear plane. Zeta potential is a measure of the potential at the shear plane. When voltage is applied to the particles, Stern layer and parts of its diffuse layer move to the opposite charge electrodes. The parts left behind of the double layers determine the zeta potential [52-60].

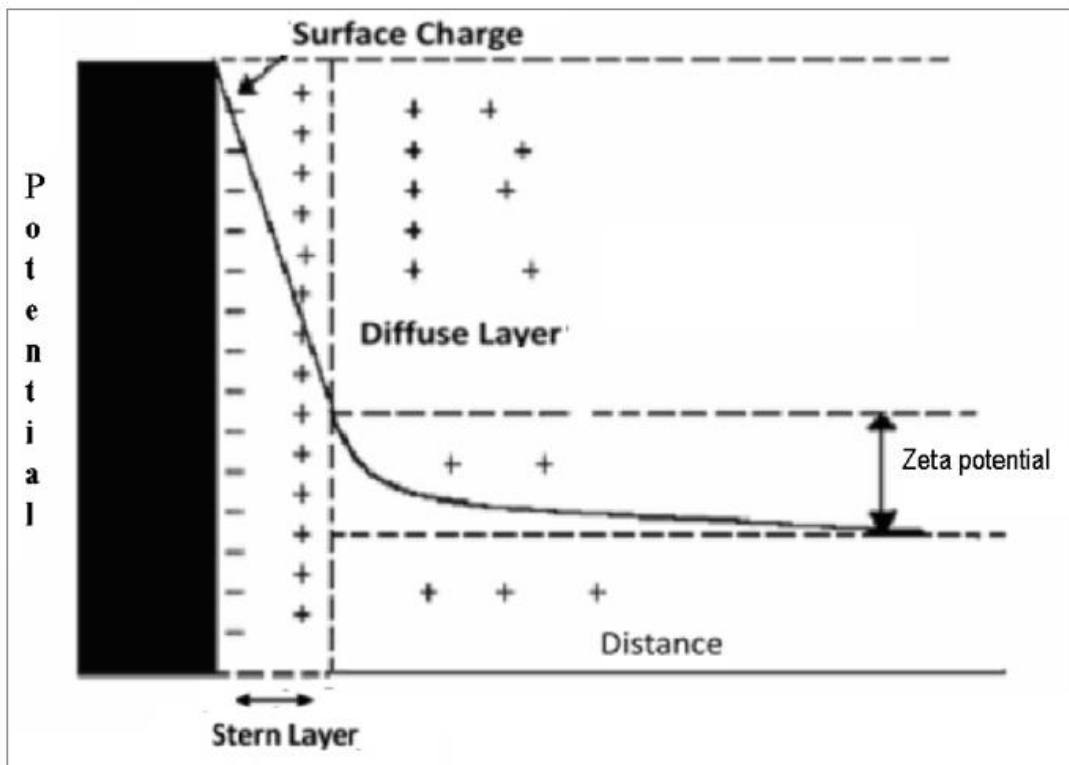


Figure 4.5: Simplified model of the electrical double layer. The Zeta potential is the electrical potential measured at the shear plane [61].

Zeta potential calculations done according to Smoluchowski formula;

$$UE = \varepsilon \zeta / \eta \quad (4.5)$$

Here UE is; applied electric potential, ε : dielectric constant, ζ : zeta potential and η : viscosity of dispersion [59].

4.3 Magnetorheology

Magnetorheological suspensions show a transition from a liquid behavior to a solid when magnetic field is applied. Because of the applied magnetic field magnetizes particles that have attractive dipolar forces between them aggregates. Hence the phase transition from liquid to solid phase. The basic phenomenon in magnetorheology is the ability to control the structure of a biphasic fluid. The two phases are composed of solid particles and their carrier fluids. The application of a magnetic field induces aggregation of the magnetic particles, hence an increase of the viscosity. All these materials have common features regarding the relation between the shape and size of the domains of the dispersed phase and their rheology. Even the interactions between the dispersed particles can be very different depending on their size (polymer, nanoparticle, etc.), conductivity, permittivity, magnetic permeability, properties of the interface and so on. Briefly, magnetorheometers are used for studying the changes in flow properties that occur in fluids which are exposed to controlled magnetic fields [62-64].

5. BIOPOLYMERS

Biopolymers are promising candidates for applications in the medical field because of their versatility, biocompatibility, bio absorbability and non-toxicity. Latest popular polymers in medical fields include new capability polymers like alginate, chitin/chitosan, cellulose, hydro gels, hydrocolloids, superabsorbent polymers and such others. Biopolymers are usually biodegradable and non-toxic polymers produced from natural sources. Biopolymers are a safer and better alternative to traditional plastics, which are petroleum-based. These polymers can be produced chemically from biological starting materials like sugars, starch, natural fats or oils, etc., or from biological systems systems like microorganisms, plants and animals. Four main types of biopolymers are based on starch, sugar, cellulose and synthetic materials [64-70].

5.1 Cellulose

Cellulose is a biopolymer that has monomeric units of sugars, amino acids and nucleotides. Cellulose is primarily defined as the non-branched macromolecule containing chain of variable lengths (Figure 5.1). The length of these chains are determined by the source of cellulose different .Generally most of natural cellulosic fibers contain 60–70% cellulose that is primarily composed of C, H, and O₂, having a general formula of C₆H₁₀O₅. But most wood fiber sourced biopolymers has a cellulose composition of 40-47% [62-65].

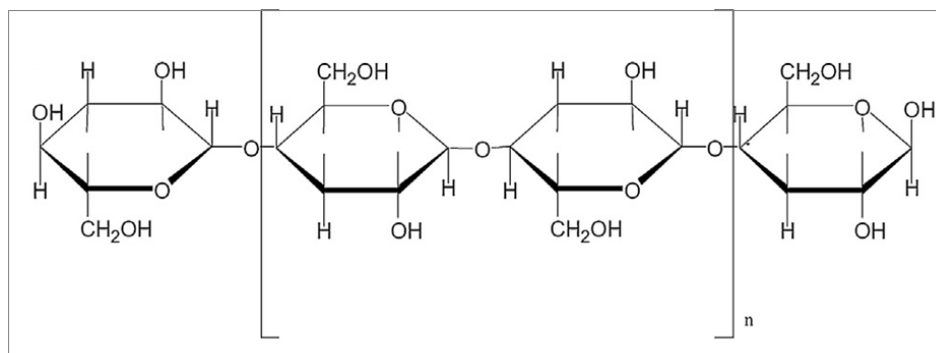


Figure 5.1: Chemical structure of cellulose [69].

5.2 Medical Applications of Biopolymers

Many of biopolymer applications can be found in the medical fields such as drug delivery systems, wound closure, healing products, and surgical implant devices , etc. biopolymers have provided a strategy for the functionalization by modulating physical and chemical properties (surface charge, etc.) improving the encapsulation, stability, and protection of drugs and nanoparticles. The recent development of nanotechnology and the various processes of functionalization of biopolymers have increased and improved its functionality as drug carrier [66, 67].

6. EVALUATIONS OF TOXICITY (IN VITRO)

Non- functionalized iron oxide nanoparticles approved for clinical use display a variety of sizes that affect their distribution within the body. Once in the body, the iron of the MNPs core is stored in the red blood cells and, like the endogenous iron, the coating of the MNP's decreases storage rate and it is eliminated via kidneys. However, the MNPs interact with different biological systems in the body and may have adverse effects. Evaluating the toxicological effects of MNPs both *in vitro* and *in vivo* is crucial for the development of MNPs-derived applications in medicine.

in vitro experiments are methods that performed in a laboratory vessel or other controlled experimental environments rather than within a living organism or natural setting. This method provides controlling of the environment and assesment at e cellular level. On the other hand, *in vivo* experiments occur within a living organism or natural setting, which gives information of sistematic interactions. The biological response of an organism to exposure of toxicants starts with toxicant induced changes at the cellular and biochemical levels, leading to changes in the structure and function of the cells, tissues, physiology and behavior of the organism. Having insight about toxicant effects at cellular level is important for designing desired drug models and to screen designed drugs adverse effects [71]. Mammalian cell interactions would give a good insight to whether MNPs functionalized with biopolymers have drug potential or not.

7. EXPERIMENTAL SECTION

Iron oxide samples were dispersed in distilled water with ultrasonic bath at different solid loadings. Concentration unit of every prepared sample is weight/volume percent (w/v). The Fe_2O_3 dispersions were mixed with different concentrations of HEC or NC between the range of 10^{-5} to 1 g/L. The polymers were dissolved in distilled water (dH_2O). Then, the dispersions were shaken and ultrasonicated for 5 min. Later Doxorubicin was loaded to biopolymer-MNP structures with the method described in section 7.7.4 and cancer cell toxicity of DOX loaded particles were evaluated.

7.1 Characterization of MNPs

Characterization provides an opportunity to analyze the results of experiments and to choose the next step to achieve expected results. Characterization techniques are required to determine magnetic nanoparticle properties such as size, crystal structure, material's thermal stability, absorption spectrum and magnetic behavior. Characterization of nanostructured materials is important because human eye cannot determine such small structures and their properties.

A scanning electron microscope (SEM) is used to determine the size, morphology, and qualitative chemical composition of the iron oxide nanoparticles with or without biopolymers. SEM scans an electron beam across the entire sample and the signal created from electron-sample interaction creates the image [72].

X-ray diffraction (XRD) gives information about crystal structure of magnetic nanoparticles. Measurements are performed with samples prepared on glass slides at room temperature. The elastically scattered or Bragg diffracted x-rays are measured in the detector. The sample and the detector are rotated at θ and 2θ respectively to obtain diffraction data of the entire sample [73, 74].

Fourier transform infrared spectroscopy (FTIR) measurements are performed to analyze the chemical bonds and functional groups of samples. In FTIR, the incident

infrared (IR) beam is first resolved into its individual frequency components via an interferometer. The infrared (IR) beam resolved into its individual frequency components induces vibrational excitations in sample atoms of the sample. The detector measures the IR signal after interaction with the sample. A Fourier transform of this signal gives the final IR spectrum in terms of transmission or absorption. The spectrum shows the characteristic vibrational frequencies of the sample. These results provide information about sample chemical composition and the surface functional groups [75].

Thermogravimetric analysis (TGA) is an analytical technique used for determination of material's thermal stability and monitoring the weight change that occurs when specimen is heated. Measurements are usually carried out in air or in an inert atmosphere and the weight change is recorded as temperature increases. In addition to weight changes, some instruments (differential thermal analysis or DTA) also record the temperature difference between the specimen and one or more reference pans. TGA gives quantitative measurements of mass changes related to dissociation of bonds, oxidation, surfactant layer, or decomposition of the sample. These measurements can also be used for determination of the volatile content in the sample [76].

Vibrating Sample Magnetometers (VSM) are used to measure the magnetic properties of materials as a function of magnetic field, temperature, and time. If a material is placed within a uniform magnetic field, generated by an electromagnet or a superconducting magnet, induction of magnetic moment is observed. In a VSM, particles made to undergo sinusoidal motion generates magnetic flux changes which is sensed by sensing coils and these sensed signals provide results of magnetic moment of the sample [77].

7.2 Materials and Methods

In this study, the main goal is to prepare biopolymer coated superparamagnetic iron oxide nanoparticles that can allow drug delivery to tumor tissue by magnetic manipulations. Polymer coated superparamagnetic iron oxide nanoparticles were synthesized to obtain a biocompatible anticancer nanodrug model. Iron oxide (Fe_2O_3) nanoparticles were purchased from Sigma–Aldrich Co (544884) and used without further purifications. Biopolymer used for experiments were 2-Hydroxyethyl

cellulose (HEC) and Nanocrystalline Cellulose (NC). HEC (Figure 7.1) was purchased from Sigma–Aldrich Co and NC was produced from wood fibers by Ayse Alemdar [78].

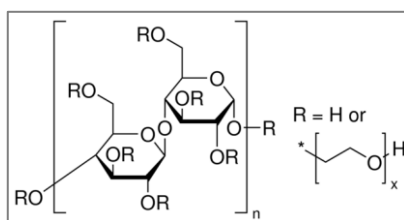


Figure 7.1 :Chemical structure representation of HEC [78].

7.3 Properties of Iron Oxide Particles

7.3.1 Rheological and electrokinetical properties

Iron oxide samples were dispersed in distilled water with ultrasonic bath at different solid loadings. Rheological properties such as viscosity, shear rate ($\dot{\gamma}$) and shear stress (τ) of dispersions were measured using a Brookfield DVIII + type low-shear viscometer. The flow behavior of the clay dispersions was obtained by shear rate measurements within 0 to 330 s^{-1} shear rates. Rheological measurements were carried out in duplicate. All the measurements were performed at natural dispersion pH levels. The rheological properties of different Fe_2O_3 concentrations were examined and flow models of the dispersions were determined from their flow curves (Figure 7.2).

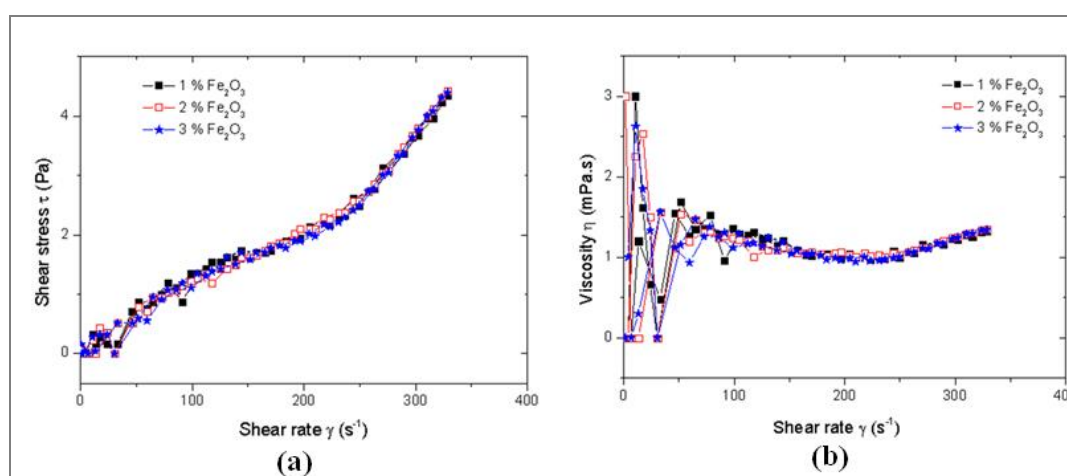


Figure 7.2 : Flow behavior: (a) Flow curves. (b) apparent viscosities of Fe_2O_3 dispersions with different concentration.

All Fe₂O₃ dispersions showed Non newtonian-type, shear thickening (Dilatant) flow behavior. In this type of flow, the very act of deforming a material can cause a rearrangement of its microstructure such that the resistance to flow increases with any increase in shear rate. In other words, the viscosity increases with applied shear rate and the flow curve can be fitted with the power law;

$$\sigma = k\dot{\gamma}^n \quad (7.1)$$

where $n > 1$ (shear thickening) flow behavior. As seen on Figure 7.2 increasing Fe₂O₃ concentration does not have a major effect on the flow behavior of Fe₂O₃ dispersions. The change of the apparent viscosity of the dispersions is given in Figure 7.2 as a function of the shear rate. Rheological properties of Fe₂O₃ dispersions do not show major differences as concentration changes, so 2% Fe₂O₃ dispersions were chosen to be used for further studies because other concentrations (1% and 3%) are too dilute or concentrated for further experiments.

The electrophoretic mobility measurements were carried out using a Zetasizer 2000, Malvern Instruments. The optic unit contains a 5mW He-Ne (638 nm) laser. The dispersions were prepared as explained above. Before the measurements, all dispersions were centrifuged at 4500 rpm for 30 min. Supernatants were then used for zeta potential measurements. To make an electrophoretic mobility measurement in this instrument, laser beams are crossed at a particular point in the cell. Particles in the cell were illuminated by these beams. Electrophoretic mobility was measured, injecting a small portion of the dispersion into the cell of the Zetasizer 2000 instrument at 25⁰C temperature. The electrophoretic mobility was then converted to zeta potential using Henry equation.

Zeta potential value of Fe₂O₃ particles was measured as -18.6mV. This value indicates that the particles tend to flocculate in the dispersion [79]. The interaction of particles with each other and the solvent molecules are less than the gravitational force, so the particles tend to fall down to the bottom of the tube.

7.4 Synthesis of Biopolymer Coated Superparamagnetic Iron Oxide Nanoparticles

The Fe₂O₃ dispersions were mixed with 10⁻⁵ to 1 g/L at different concentrations of HEC or NC. The polymers were dissolved in distilled water (dH₂O). Then, the

dispersions were shaken and ultrasonicated for 5 min. Rheological and electrokinetical properties of the dispersions were determined to find out the proper concentrations of each polymer, which covers the whole surfaces of the Fe_2O_3 particles' surface.

7.5 Interactions with HEC and Fe_2O_3

7.5.1 Rheological properties

Influences of biopolymers upon the Fe_2O_3 dispersions and their rheological properties were examined. Flow curves and apparent viscosities are measured to determine the effects of polymers on 2% Fe_2O_3 dispersions. Effect of HEC on Fe_2O_3 dispersions and their rheological properties are shown in Figure 7.3.

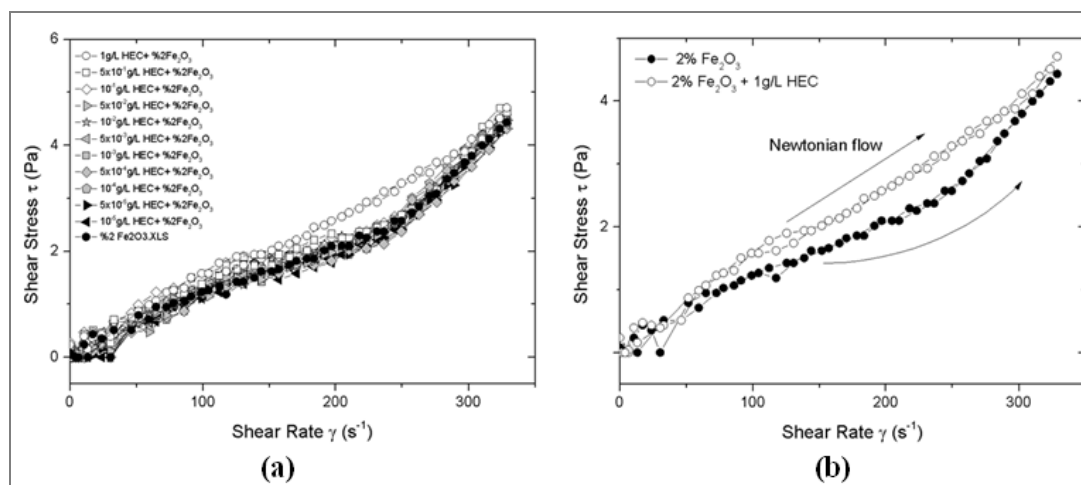


Figure 7.3: Shear stress-shear rate graphs of: (a) all HEC concentrations with 2% Fe_2O_3 dispersions. (b) 1g/L HEC+2% Fe_2O_3 and 2% Fe_2O_3 dispersions.

The HEC polymer attached to the some part of the Fe_2O_3 surfaces and reduced the interactions between the ironoxide particles. HEC prevented the rearrangement of the particles, as a result the flow regimes changed to the non-interacting regime which is called Newtonian flow. The flow curves of the HEC added samples were given in the Figure 7.3.

Because of the different flow regimes, the apparent viscosity values at different speeds were used to determine the correlation between the solutions. Figure 7.4 shows the changes of the apparent viscosity values of dispersions at different speeds of the rheometer. Figure 7.4 shows the change of apparent viscosity versus increasing HEC concentration. According to the figure, HEC did not change the

viscosity of the medium. The last points at apparent viscosity-HEC concentration graph indicated the slight increment of the viscosity but indeed it was the viscosity increment of the polymer solution. The viscosity values slightly increased with increasing speed especially at 250 rpm. Shear thickening behavior of Fe_2O_3 should be the reason of the increasement.

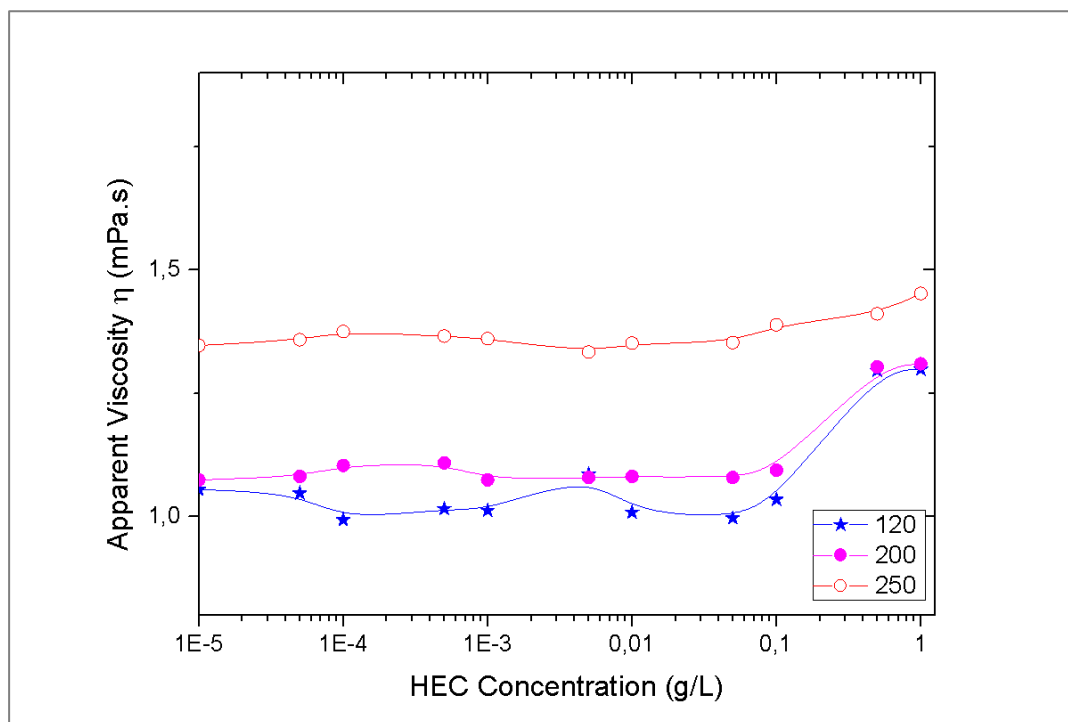


Figure 7.4: Apparent viscosity -HEC concentration graphs for all 2% Fe_2O_3 dispersions with different HEC concentrations. Apparent viscosities were measured at different speeds (120,200,250) of rheometer.

7.5.2 Electrokinetical measurements

The zeta potential measurements were carried out for all 2% Fe_2O_3 and 2% Fe_2O_3 +HEC dispersions with different biopolymer concentrations within the range of 1×10^{-5} to 1 g/L. Before the measurements all the dispersions were centrifugated at 4500 rpm for 10 min then their supernatants were used for measurements. In Figure 7.5, the zeta potential of 2% Fe_2O_3 +HEC dispersions is plotted as a function of increasing HEC concentrations. The zeta potential value of the 2% Fe_2O_3 dispersion in the absence of HEC was measured to be -18.6 mV. Zeta potential values of the dispersions up to 0.01 g/L HEC concentrations were in a decreasing regime, but further increase in HEC concentrations resulted in positive zeta potentials. This indicates that positively charged HEC molecules are attach to the negatively charged Fe_2O_3 nanoparticles and covered the whole surface of the particles. The zero point of

charge of the 2%Fe₂O₃+HEC dispersions was measured at ~0.05 g/L polymer concentrations.

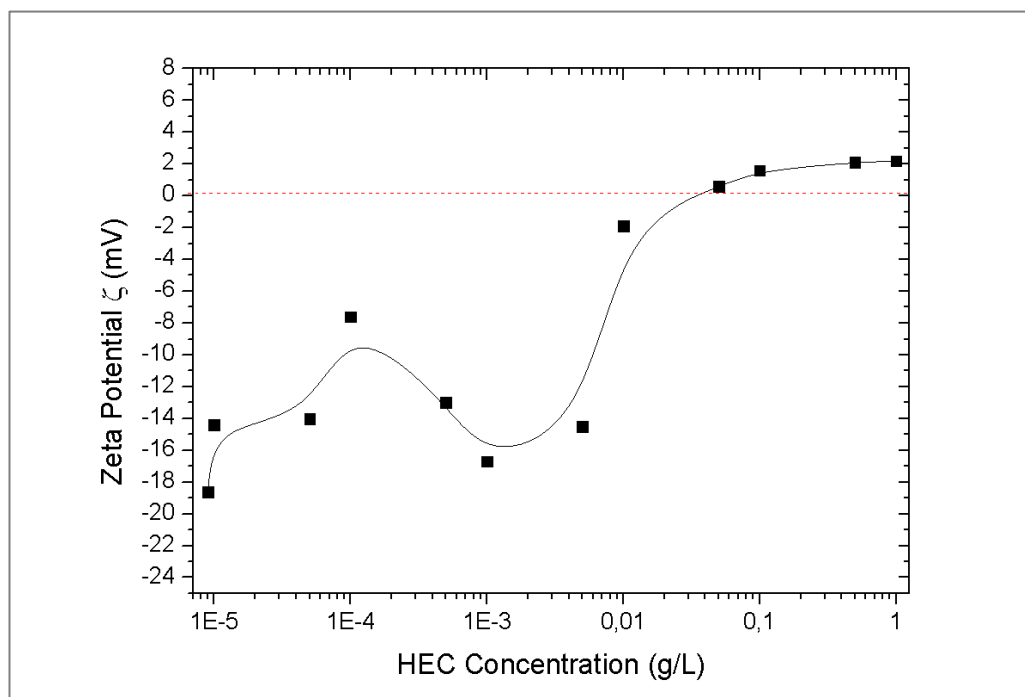


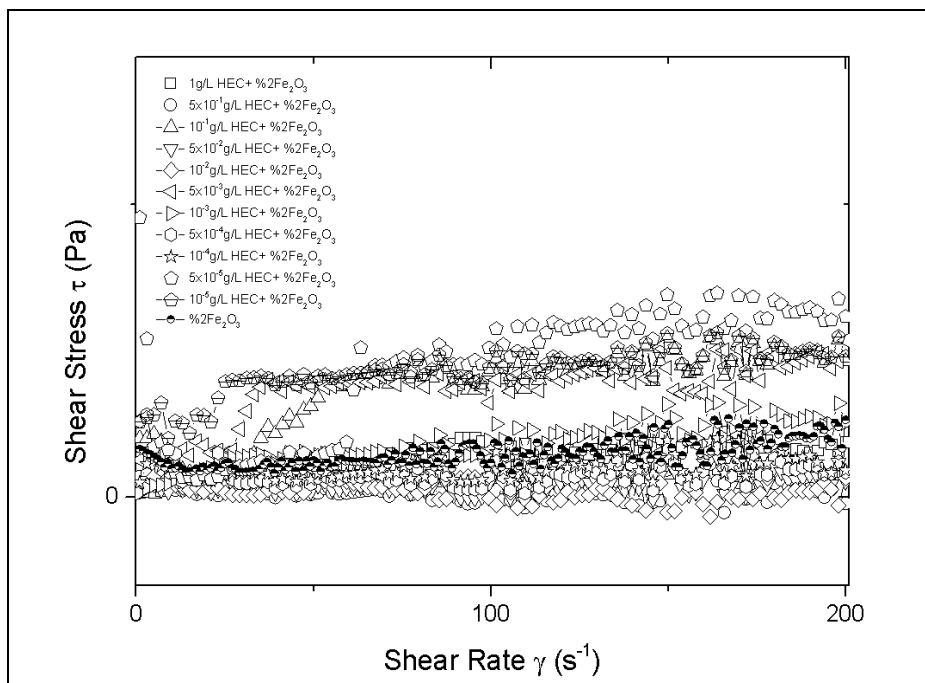
Figure 7.5: Zeta potential of 2% Fe₂O₃+HEC dispersions as a function of increasing HEC concentration.

7.5.3 Magnetorheology

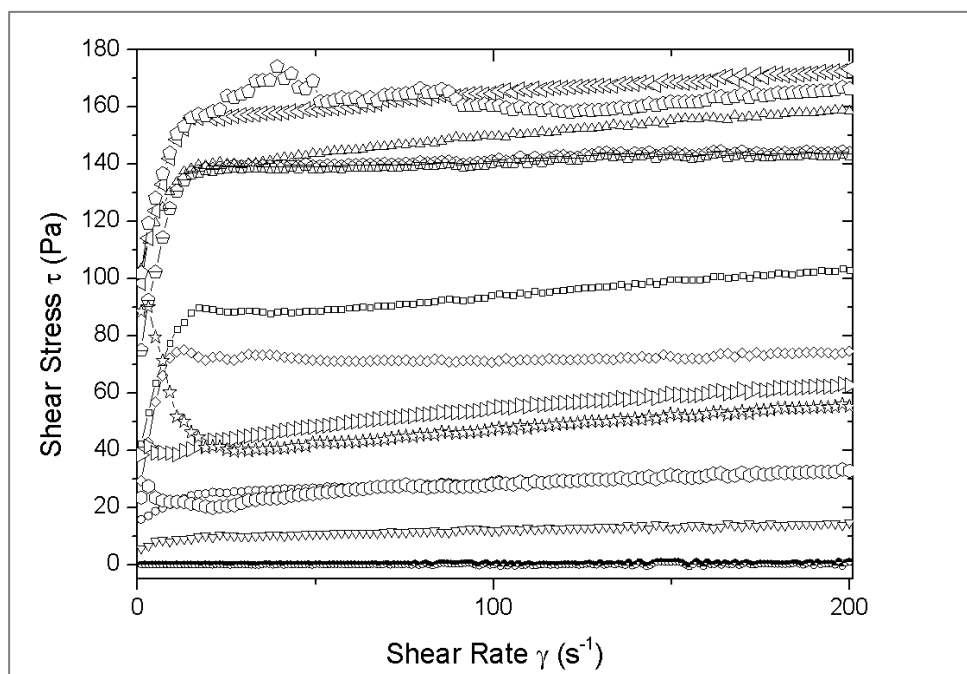
A Magneto Rheological Device (MRD 180, Anton Paar Companies, Germany) was used for determining the effect of a magnetic field on the rheology of magnetic fluids (Fe₂O₃ dispersions). Different magnetic fields were applied on each sample and the effect of magnetic field on sample dispersions flow behaviour, apparent viscosity, shear stress and shear rate was examined. In the following test, the test currents were 0A to 1A with and the intensities of magnetic fields were 0 mT 220 mT.

In the magnetorheometer, only the lower plate can apply the magnetic field. Hence, when we applied the magnetic field, the particles stuck to the lower plate and the water in the dispersion released. If we performed the measurement at this condition, the rheological parameters would only belong to the released water. Therefore, the water on the rheometer were removed in controlled manner before the measurements. In this case the rheological parameters of the dispersions changed compared to the results of section 7.5.1. The flow curves of the water-removed dispersions were given in Figure 7.6 The magnetic field applied to the same dispersions to compare the magnetorheological effects.

The viscosity decrease can be seen in Figure 7.6 as polymer concentration changes. This indicates that polymers lower the interaction between Fe_2O_3 particles, which changes flow behaviour and decreases viscosity. This property gained by adsorbing polymers to Fe_2O_3 surface.



(a)



(b)

Figure 7.6: Shear stress plotted as a function of shear rate: for suspensions containing different concentrations of HEC under test currents (a) 0A. (b) 1A.

The viscosity decrease can be seen in Figure 7.6 as polymer concentration changes. This indicates that polymers lower the interaction between Fe_2O_3 particles, which changes flow behaviour and decreases viscosity. This property gained by adsorbing polymers to Fe_2O_3 surface.

7.5.4 Fourier transform infrared spectroscopy (FTIR)

FTIR spectrum measurements were performed in both transmittance and absorbance modes using the Perkin Elmer Spectrum One Spectrophotometer (wavelength range of $400\text{--}4000\text{ cm}^{-1}$). Each sample of Fe_2O_3 and Fe_2O_3 in the presence of different HEC concentrations (in the solid state) were mixed with KBr with a sample ratio of %0.1 weight/weight % (w/w %) and ground very finely with an agate pestle and mortar. After each KBr and sample mixture was compressed into a KBr pellet (under ~ 10 tons for ~ 2 min) for FTIR spectroscopy measurements.

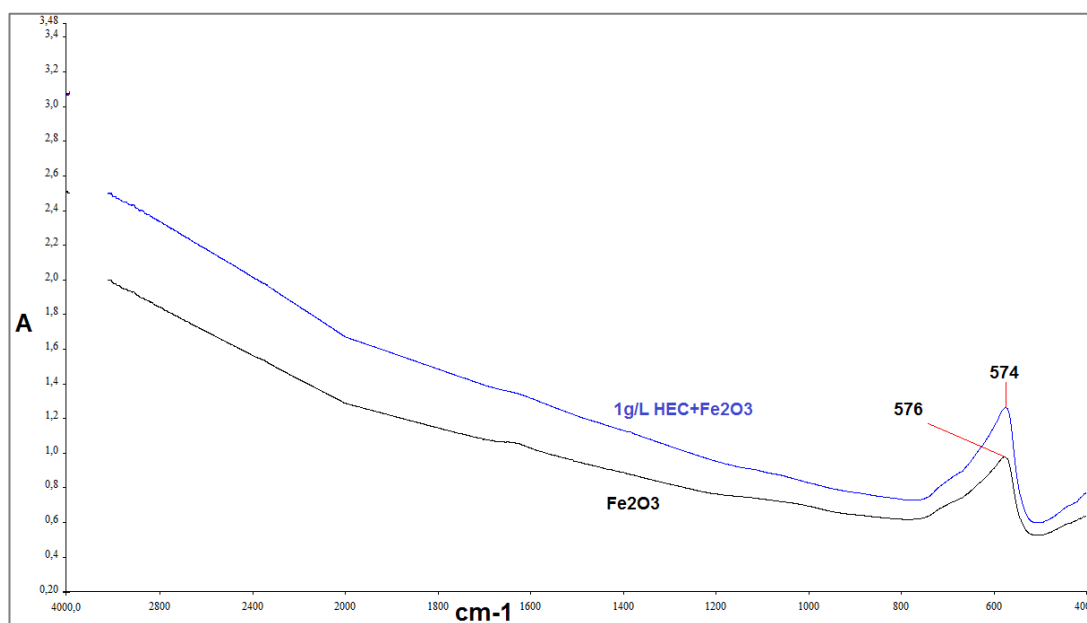


Figure 7.7: FTIR spectrum of Fe_2O_3 and 1g/L HEC+ Fe_2O_3 .

Characteristic Fe-O stretching vibration peak was determined at 576 cm^{-1} for Fe_2O_3 . The results showed that addition of the polymer HEC did not change the spectrum of Fe_2O_3 (as seen on Figure 7.7).

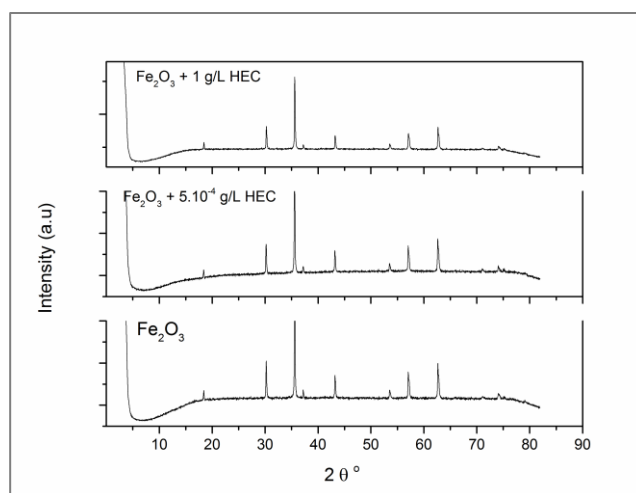
The characteristic Fe-O vibration peaks were shifted slightly with addition of the polymer HEC as seen in Table 7.1. The reason for this shift was overlapping of HEC and Fe_2O_3 peaks. No binding peaks were observed as expected.

Table 7.1: Fe-O stretching vibration peak values for different concentrations of HEC.

Concentration	Fe-O stretching vibration peak (cm^{-1})
2% Fe_2O_3	576
10^{-5} g/L HEC+ 2% Fe_2O_3	583
5×10^{-5} g/L HEC+ 2% Fe_2O_3	574
10^{-4} g/L HEC+ 2% Fe_2O_3	572
5×10^{-4} g/L HEC+ 2% Fe_2O_3	579
10^{-3} g/L HEC+ 2% Fe_2O_3	575
5×10^{-3} g/L HEC+ 2% Fe_2O_3	577
10^{-2} g/L HEC+ 2% Fe_2O_3	573
5×10^{-2} g/L HEC+ 2% Fe_2O_3	578
10^{-1} g/L HEC+ 2% Fe_2O_3	571
5×10^{-1} g/L HEC+ 2% Fe_2O_3	572
1 g/L HEC+ 2% Fe_2O_3	574

7.5.5 X-Ray diffraction analysis (XRD)

The crystal structure of Fe_2O_3 and Fe_2O_3 in the presence of HEC was measured by X-Ray diffraction analysis using Philips PW1040. Each sample was prepared by covering glass slides with sample suspensions and leaving them to dry at room temperature. Figure 7.8 shows the XRD patterns of the Fe_2O_3 samples with and without HEC. According to these results, no changes were determined as HEC concentration changes.

**Figure 7.8:** X-ray diffraction patterns of Fe_2O_3 , 5×10^{-4} g/L HEC+ 2% Fe_2O_3 and 1 g/L HEC+ 2% Fe_2O_3 .

7.5.6 Scanning electron microscope (SEM)

Scanning electron microscopy (SEM) images of the samples were used for characterization of the dispersions with the polymer effect (Figure 7.9). Direct evidence of surface modification of the dispersion can be found in SEM examination.

SEM images of all Fe_2O_3 nanoparticles and HEC biopolymer coated Fe_2O_3 nanoparticles were obtained for particle size determination and imaging. The morphology of the fractured surfaces of the samples was investigated with a FEI Quanta Feg 250 scanning electron microscope. SEM measurements were operated at 15 kV. The specimens were frozen under liquid nitrogen, and then fractured, mounted, and coated with gold on Edwards S 150B sputter coater.

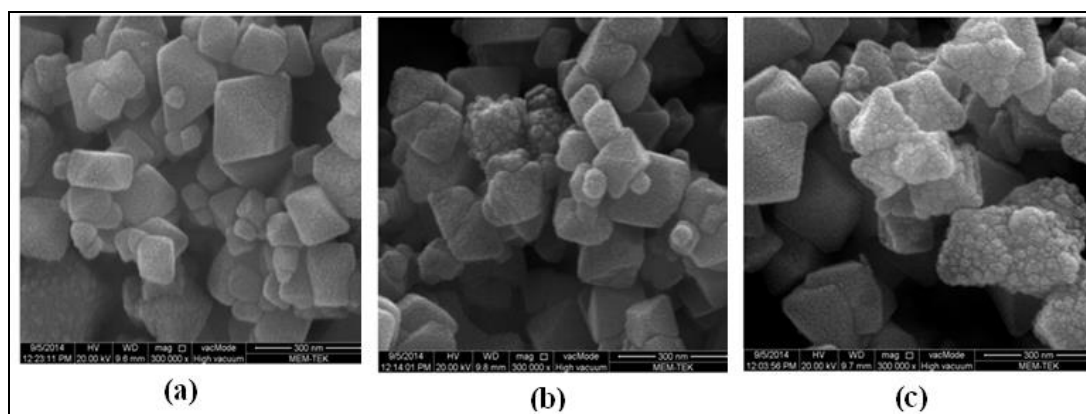


Figure 7.9: SEM images of (a) 2% Fe_2O_3 , (b) 5×10^{-4} g/L HEC + 2% Fe_2O_3 , (c) 1 g/L HEC + 2% Fe_2O_3 respectively.

HEC polymer appeared on the ironoxide particles as dotted texture. The increasing concentration of HEC polymer increased the number of coated Fe_2O_3 particles as seen on the SEM pictures.

7.6 Interactions with NC and Fe_2O_3

7.6.1 Rheological properties

Influences of NC biopolymer upon the Fe_2O_3 dispersions, their rheological properties and flow behaviours were examined. Shear stress, shear rate and apperent viscosities of all 2% Fe_2O_3 dispersions with different NC concentrations are measured to determine the effects of polymers on Fe_2O_3 nanoparticles.

Effect of NC on Fe_2O_3 dispersions and their rheological properties are shown in the figures given below. The flow curves of the NC added samples at all concentrations were given at the Figure 7.10 and the differences between the flow curves of Fe_2O_3 and 1 g/L NC added Fe_2O_3 samples were given at Figure 7.10. These results indicated that NC polymer is attached to some part of the Fe_2O_3 surfaces and reduced the interactions between the iron oxide nanoparticles and changed its flow behavior by preventing rearrangement of Fe_2O_3 nanoparticles. As it can be seen in Figure 7.10 at

1g/L NC biopolymer concentrations there is a change in flow behavior compared to 2% Fe_2O_3 .

NC polymer prevented the rearrangement of the particles (similarly like HEC) so as a result the flow regimes changed to the non-interacting regime, which is called Newtonian flow.

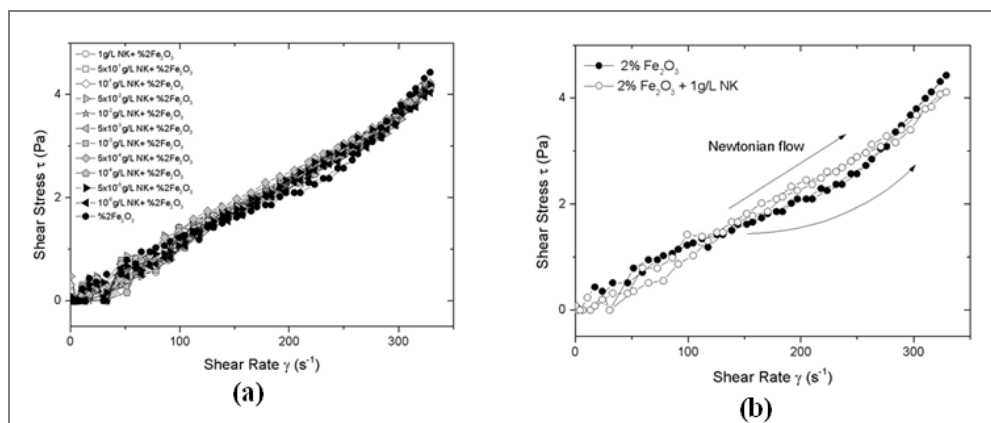


Figure 7.10: Shear stress-shear rate graphs of: (a) all NC concentrations with 2% Fe_2O_3 dispersions. (b) 1g/L NC+2% Fe_2O_3 and 2% Fe_2O_3 dispersions.

Because of the different flow regimes, the apparent viscosity values at different speeds were used to determine the correlation between the solutions. Figure 7.11 shows the changes of the apparent viscosity values of dispersions at different speeds of the rheometer.

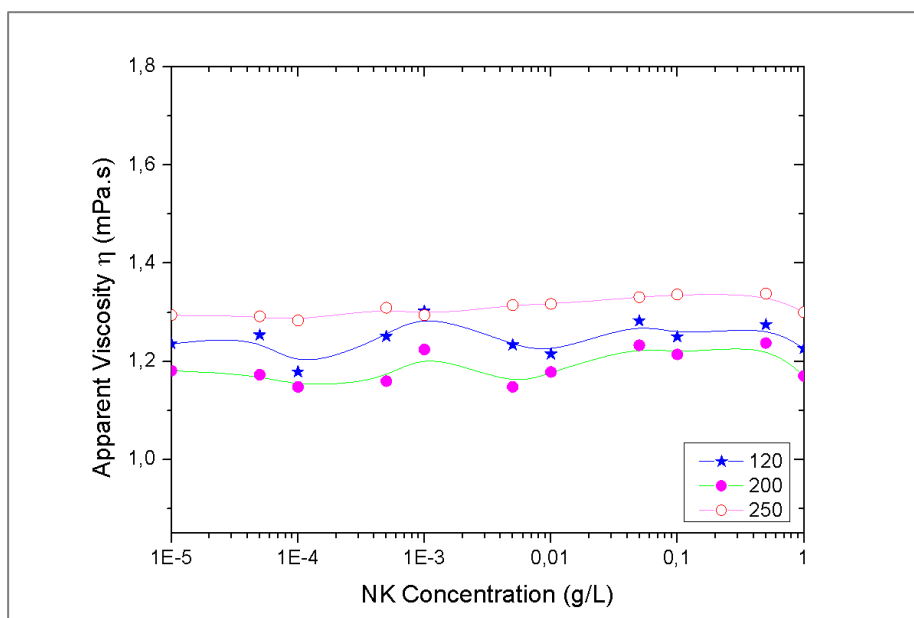


Figure 7.11: Apparent viscosity-NC concentration graphs for all 2% Fe_2O_3 dispersions with different NC concentrations. Apparent viscosities were measured at different speeds (120,200,250) of rheometer.

7.6.2 Electrokinetical measurements

The zeta potential measurements were carried out for all 2% Fe_2O_3 and 2% Fe_2O_3 +NC dispersions with different biopolymer concentrations within the range of 1×10^{-5} to 1 g/L. Before the measurements, all the dispersions were centrifugated at 4500 rpm for 30 min, then their supernatants were used for measurements. In Figure 7.12, the zeta potential of 2% Fe_2O_3 + NC dispersions is plotted as a function of increasing NC concentrations. The zeta potential value of the 2% Fe_2O_3 dispersion in the absence of NC was measured to be -18.6mV. There was only a plateau on the zeta potential of the dispersion up to 0.1 g/L NC concentrations but further increase in NC concentrations resulted in increasing zeta potentials. While positive zeta potentials were reached using HEC, zero point could not be reached for NC biopolymer concentrations. This indicates that positively charged NC molecules are still attached to the negatively charged Fe_2O_3 nanoparticles and covered their surfaces but only partially.

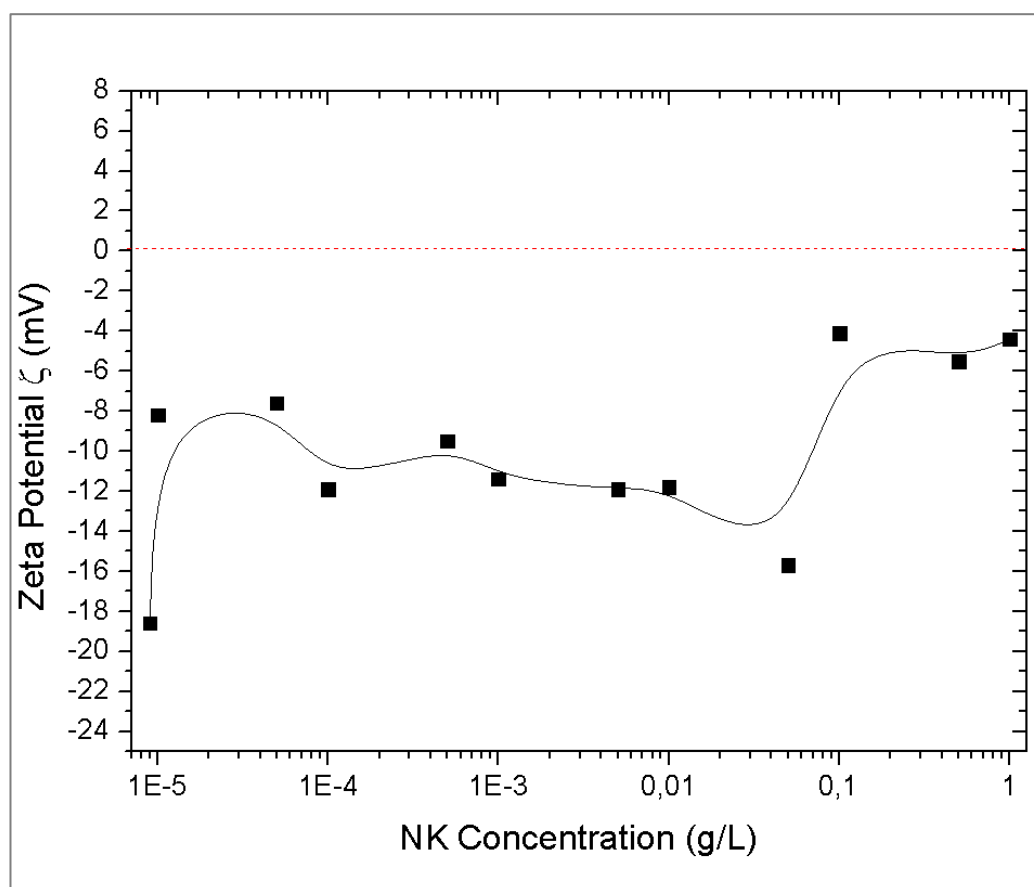
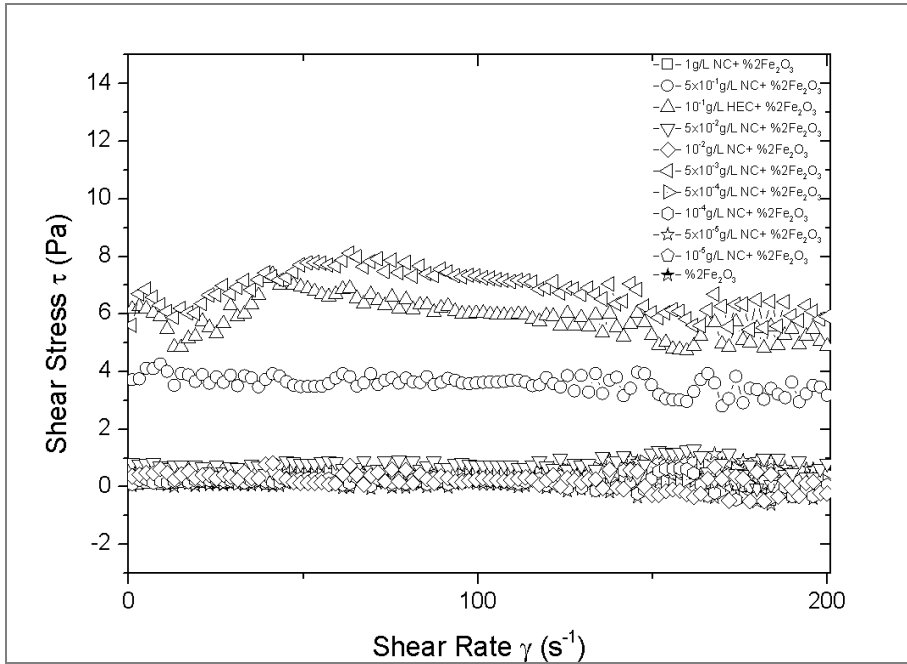


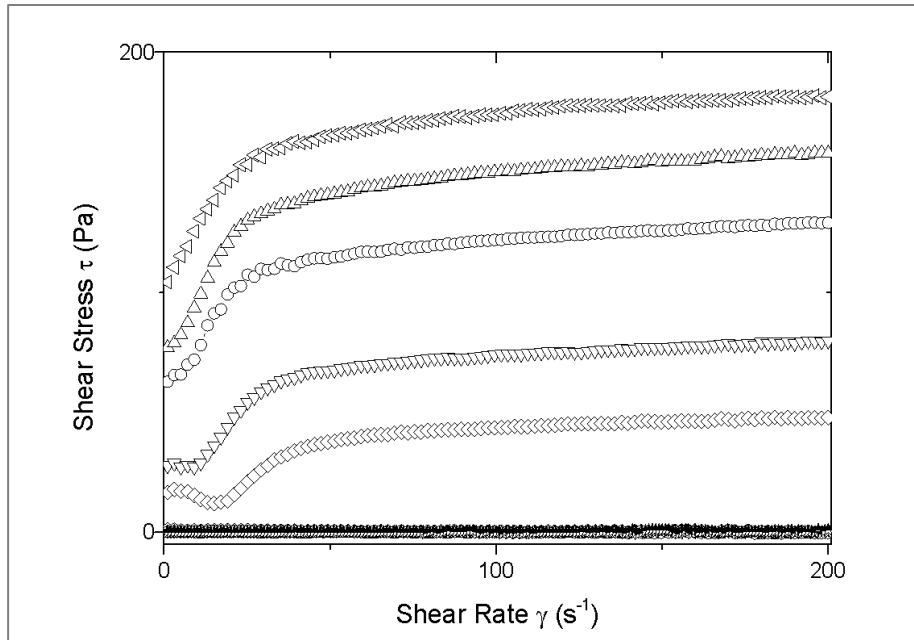
Figure 7.12: Zeta potential of 2% Fe_2O_3 + NC dispersions as a function of increasing NC concentration.

7.6.3 Magnetorheology

Experiments were performed under same conditions as descibed in section 7.5.3 Different magnetic fields were applied on each sample of 2% Fe_2O_3 and NC + 2% Fe_2O_3 disperions and the effect of magnetic field on these samples and their rheological properties were examined.



(a)



(b)

Figure 7.13: Shear stress plotted as a function of shear rate for suspensions containing different concentrations of NC under test currents (a) 0A. (b) 1A.

The results were similar with HEC and it can be seen in Figure 7.13 that at 1g/L polymer concentration viscosities are much lower (for both polymers) than uncoated particles.

7.6.4 Fourier transform infrared spectroscopy (FTIR)

FTIR spectrum measurements were performed in both transmittance and absorbance modes using Perkin Elmer Spectrum One Spectrophotometer (wavelength range of 400-4000 cm^{-1}). Each sample (in the solid state) were mixed with KBr with a sample ratio of %0.1 w/w and ground very finely with an agate pestle and mortar. After each KBr and sample mixture was compressed into a KBr pellet (under ~10 tons for ~2min) for FTIR spectroscopy measurements.

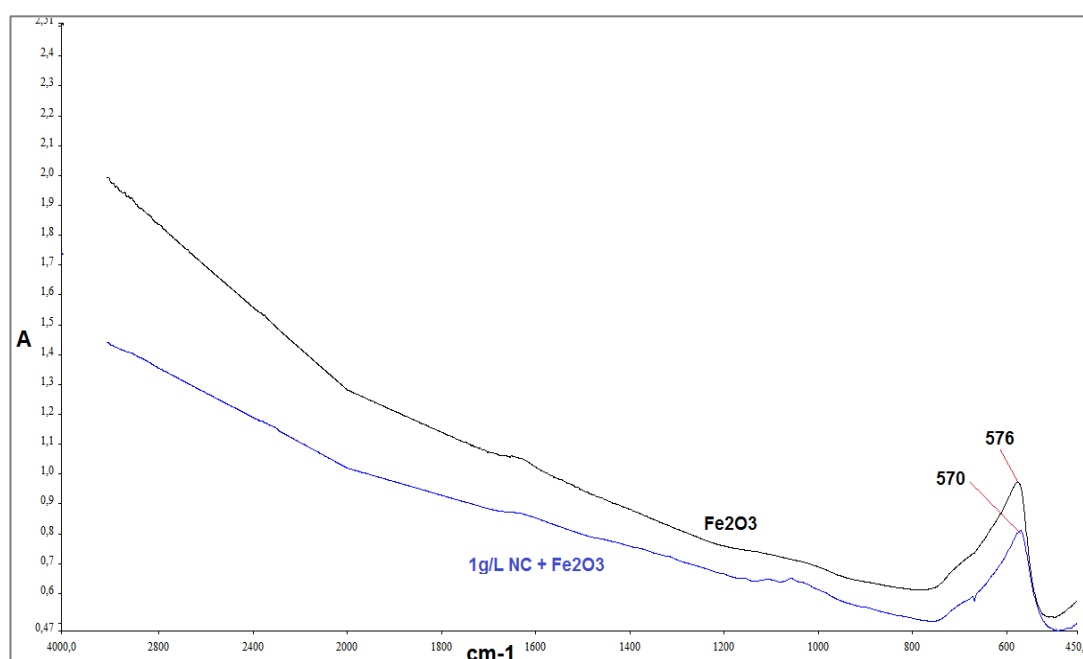


Figure 7.14: FTIR spectrum of each sample of Fe_2O_3 and Fe_2O_3 in the presence of different HEC concentrations.

We have mentioned that characteristic Fe-O stretching vibration peak was determined at 576 cm^{-1} for Fe_2O_3 (Figure 7.14). The results of NC added samples were similar to HEC added samples. FTIR examination of 1g/L NC added sample showed that addition of the polymer did not change the spectrum of Fe_2O_3 . The characteristic Fe-O vibration peaks were shifted slightly with addition of the polymer (Table 7.2.). The reason for this shift was also overlapping of NC and Fe_2O_3 peaks just like HEC did. No binding peaks were observed as expected.

Table 7.2: Fe-O stretching vibration peak values for different concentrations of NC.

Concentration	Fe-O stretching vibration peak (cm ⁻¹)
2%Fe ₂ O ₃	576
10 ⁻⁵ g/L NC+ 2%Fe ₂ O ₃	572
5x10 ⁻⁵ g/L NC+ 2%Fe ₂ O ₃	575
10 ⁻⁴ g/L NC+ 2%Fe ₂ O ₃	571
5x10 ⁻⁴ g/L NC+ 2%Fe ₂ O ₃	579
10 ⁻³ g/L NC+ 2%Fe ₂ O ₃	574
5x10 ⁻³ g/L NC+ 2%Fe ₂ O ₃	571
10 ⁻² g/L NC+ 2%Fe ₂ O ₃	572
5x10 ⁻² g/L NC+ 2%Fe ₂ O ₃	569
10 ⁻¹ g/L NC+ 2%Fe ₂ O ₃	569
5x10 ⁻¹ g/L NC +2%Fe ₂ O ₃	572
1g/L NC+ 2%Fe ₂ O ₃	571

7.7 Drug Testing

To choose the proper concentrations of the polymers which covers the whole surface of the Fe₂O₃ particle in a stable dispersion, rheological and electrokinetical data was used. Addition of HEC did not change the aggregation behavior of the dispersions but covered the whole surfaces of the iron oxide particles after the 0.05g/L HEC concentration. HEC did not change any structural properties of the iron oxide so the attachment of HEC to the Fe₂O₃ particle surfaces is completely caused by electrosteric effects. Positively charged HEC were attracted to the negatively charged surface of Fe₂O₃ and also, HEC changed the charge distribution on the Fe₂O₃ surface. Hence, the HEC particles were attached to the surface by steric effects. The electrostatic and steric effect together is called electrosteric effect.

For the further studies, we decided to use 1g/L HEC concentration because of the reasons above. Rheological and the electrokinetical behaviours of HEC were very similar only NC was not able to cover Fe₂O₃ surface as much as HEC. Due to similar results, 1g/L NC concentration was chosen to use for further studies.

7.7.1 Magnetic properties of synthesized Fe₂O₃ nanoparticles

As mentioned above 1g/L polymer concentrations of both HEC and NC biopolymers were chosen for further studies. The magnetization in a variable magnetic field and magnetic properties of Fe₂O₃ and Fe₂O₃ in the presence of biopolymer samples (in solid state) were determined by a vibrating sample magnetometer (VSM) (Pacific

Electric Motor Co.) at room temperature under DC-biased magnetization between 0 and 8000 Oe.

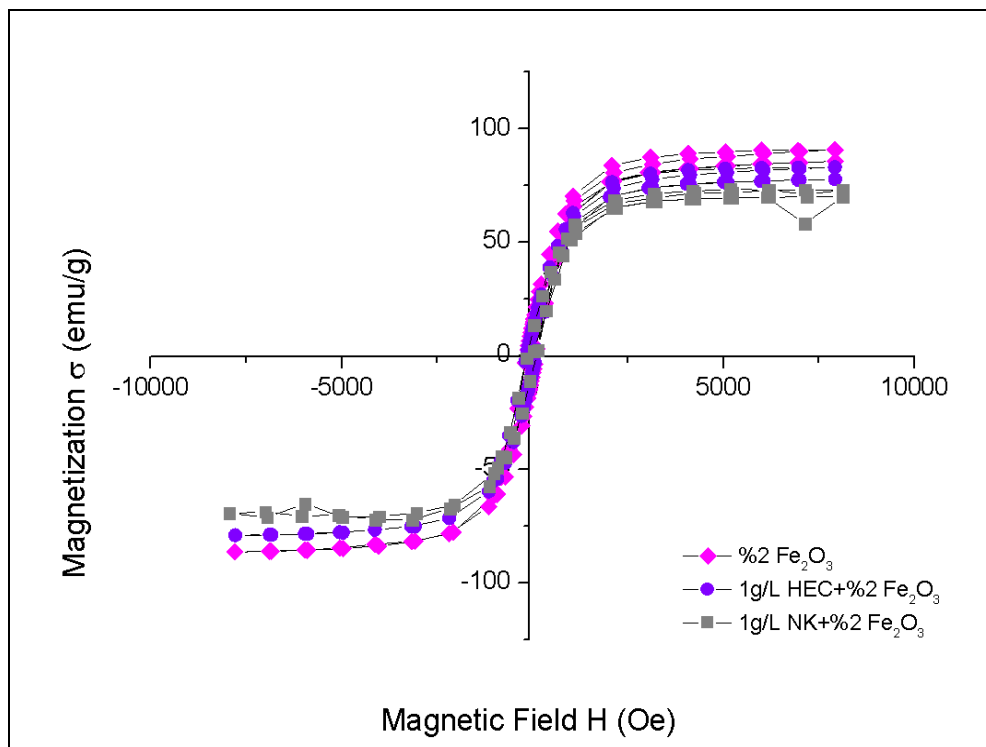


Figure 7.15: Magnetization graphs for Fe_2O_3 , 1g/L HEC+2% Fe_2O_3 , 1g/L NK+2% Fe_2O_3 .

As seen in Figure 7.15 addition of polymer to the Fe_2O_3 particles reduced the magnetization values slightly but did not change the characteristic response of Fe_2O_3 particles to the magnetic field.

7.7.2 Thermo-gravimetric and differential thermal analysis (TG/DTA) of synthesized Fe_2O_3 nanoparticles

The thermal analyses of the samples were determined using thermo gravimetric (TG) and differential thermal analysis (DTA). TG/DTA was performed in a Perkin Elmer Diamond at a heating rate of 20 °C/min under an argon atmosphere and in the temperature range of 30 and 300 °C. The results in Figure 7.16 showed that uncoated Fe_2O_3 particles gained significant amount of weight at temperatures in the range of 30 to 300 °C. This indicates that these particles were oxidized when uncoated. Coated and uncoated Fe_2O_3 particles showed different weight lost events. HEC and NC coated particles were not oxidized because of coatings prevented Fe_2O_3 particles to intreract with the environment, so, they are not oxidized and they lost weight due to the polymers weighth lost.

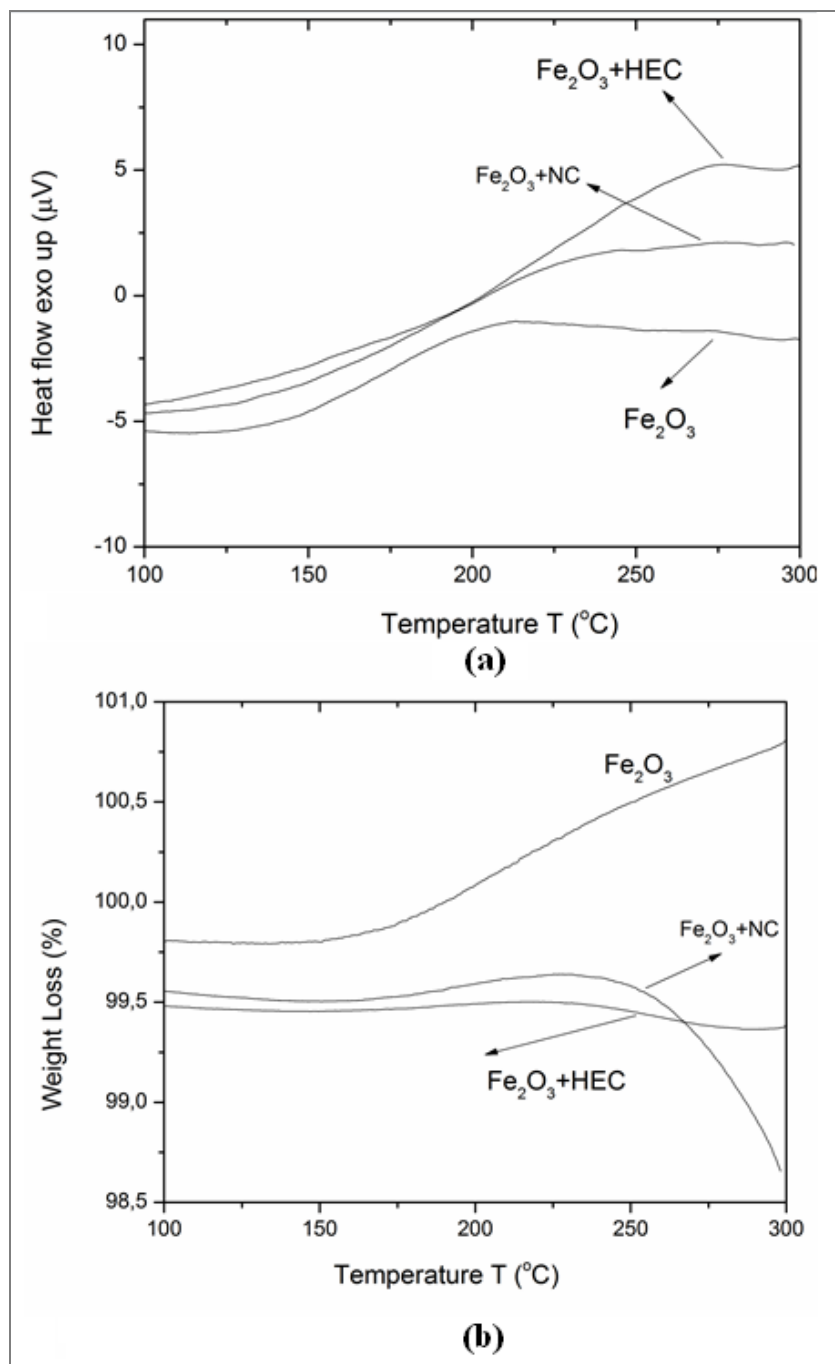


Figure 7.16: TG/DTA thermal analysis graphs: (a) TG. (b)DTA for 1g/L NC+2% Fe_2O_3 , 1g/L HEC+ 2% Fe_2O_3 , and 2% Fe_2O_3 .

The results in Figure 7.16 showed that uncoated Fe_2O_3 particles gained significant amount of weight at temperatures in the range of 30 to 300 $^\circ\text{C}$. This indicates that these particles were oxidized when uncoated. Coated and uncoated Fe_2O_3 particles showed different weight lost events. HEC and NC coated particles were not oxidized because of coatings prevented Fe_2O_3 particles to interact with the environment, so, they are not oxidized and they lost weight due to the polymers weight lost.

7.7.3 In vitro evaluations

In order to assess whether synthesized Fe_2O_3 nanoparticles could have anticancer drug potential and targeted drug delivery properties *in vitro* evaluations were performed. To examine the toxicity of synthesized Fe_2O_3 nanoparticles and DOX loaded nanoparticles cytotoxicity assays were performed for all nanoparticle samples (in solid state) using MTS [3-(4,5-dimethylthiazol-2-yl)-5-(3-carboxymethoxyphenyl)-2-(4-sulphophenyl)-2H-tetrazolium] assays. The quantity of formazan product produced by MTS was measured at 490nm with ELISA multiwell spectrophotometer (BIO-RAD Benchmark Plus). MTS was purchased from Promega (CellTiter 96® AQueous One Solution Cell Proliferation Assay). Cytotoxicity assays were applied to Human osteoblast (hFOB) and human breast adenocarcinoma (MCF7) cell lines. All cell lines were purchased from ATCC.

7.7.3.1 Mammalian cell culture

All cells were cultured in Dulbecco's modified Eagle's medium (DMEM) (HyClone, 16777-133) supplemented with 10% fetal bovine serum (FBS) (HyClone, SH3007003HI), 1% penicillin-streptomycin, 1% L-Glutamine solution. All incubations were performed in a humidified atmosphere containing 5% CO_2 at 37°C (BINDER, C150 E2). For experimental procedures all cells were detached by 0.5% Trypsin-EDTA solution (Sigma, T3924), washed two times with PBS, and resuspended in DMEM. Medium renewals of all cells were performed 2 to 3 times per week.

7.7.3.2 Cytotoxicity assays

Growth of the cell cultures were optimized before performing cytotoxicity assays. To quantitatively measure cell cytotoxicity, proliferation or viability of the nanoparticles a colorimetric MTS assay was used as mentioned above. MTS solution was stabilized by electron coupling reagent phenazine ethosulfate (PES). The quantity of formazan product measured by 490nm absorbance was subtracted from background absorbances (680nm) and assays are done multiple times for at least six wells per sample. For MTS assays, the quantity of formazan product measured is directly proportional to the number of living cells in culture so cell viability can be measured.

The relative cell viability (%) related to control wells (medium without nanoparticles) was calculated by;

$$\text{Relative cell viability (\%)} = \frac{\text{OD}_{490}}{\text{avg}(\text{OD}_{490} C')} \times 100 \quad (7.2)$$

For cytotoxicity assays hFOB and MCF7 cells were used. Cells were seeded in a 96 well plate at a density of 10,000 cells per well in 100 μL of medium. After Different concentrations (400, 250, 200, 100, 50, 25 $\mu\text{g}/\text{ml}$) of Fe_2O_3 nanoparticles (without biopolymer treatment) 1g/L NC+ 2% Fe_2O_3 and 1g/L HEC+ 2% Fe_2O_3 were prepared with DMEM supplemented with 10% FBS and added to wells. The control wells were only cultured cells in medium with no particles. Fe_2O_3 and 1g/L HEC+ 2% Fe_2O_3 treated cells in 96 well plates, cultured in DMEM supplemented with 10% FBS, were incubated for 24 h at 37 $^\circ\text{C}$ in a 5% CO_2 incubator. After 24h, MTS assays were performed by adding MTS (10% of culture medium) directly to culture wells. MTS added cultures were incubated for 4 hours then their absorbances were measured at 490nm and at 680nm (background) with a 96-well plate reader. Cell viability % of all treated cells were determined by using the formula mentioned above.

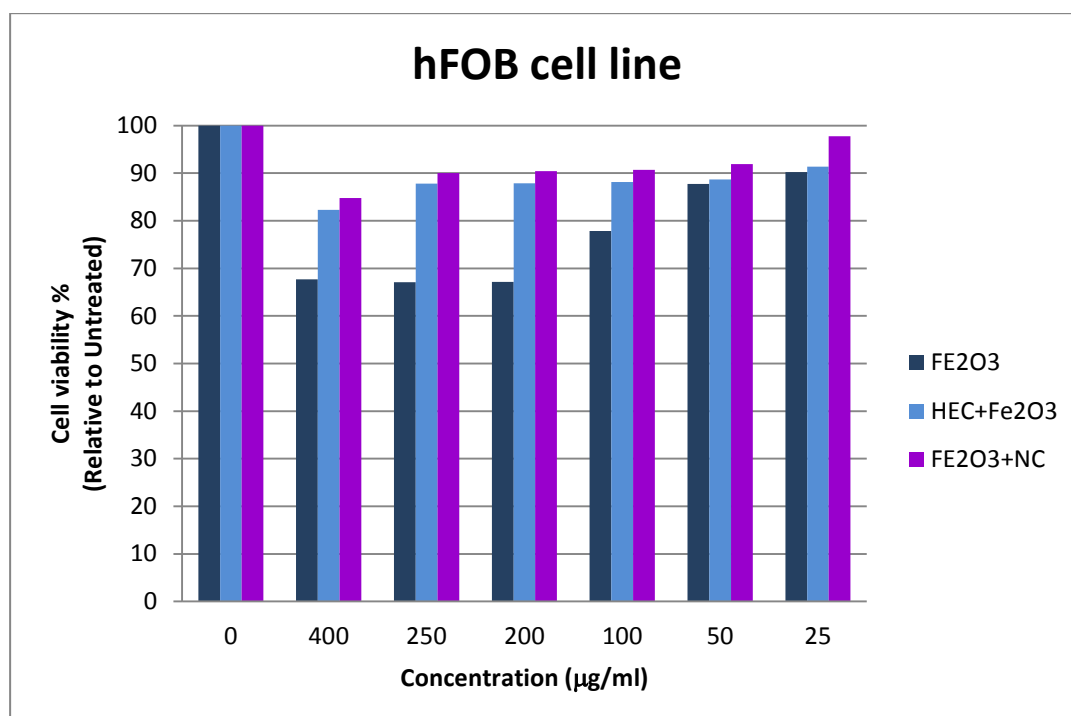


Figure 7.17: Relative cell viability (%) of hFOB treated with 1g/L HEC+2% Fe_2O_3 , for 1g/L NC+2% Fe_2O_3 and 2% Fe_2O_3 (without biopolymer treatment) dilutions (25-400 $\mu\text{g}/\text{ml}$) related to control wells.

As seen in Figure 7.17 HEC and NC coated Fe_2O_3 nanoparticle dilutions have considerably less toxicity to osteoblast cells than uncoated Fe_2O_3 dilutions. Absorbance increase at $25\mu\text{g/ml}$ measured with the MTS assay may be due to increased mitochondrial activity associated with cell phagocytosis of nanoparticles. Especially at $200\mu\text{g/ml}$ concentrations, maximum difference of cell viability can be observed. Experimental values indicate that HEC and NC coated Fe_2O_3 nanoparticles has less cell toxicity and these nanoparticles may have potential to be used as a drug targeting and delivering model with less toxicity to healthy cells like osteoblasts.

7.7.4 Doxorubicin loading to Fe_2O_3 nanoparticles

After the surface of the Fe_2O_3 nanoparticles coated with the biopolymers Doxorubicin hydrochloride (DOX; (8s-cis)-10-[(3-amino-2,3,6-trideoxy- α -l-lyxo-hexopyranosyl)oxy]-7,8,9,10-tetrahydro-6,8,11-trihydroxy-8-(hydroxyacetyl)-1-methoxynaphthacene-5,12-dione hydrochloride) purchased from Edqm (D2975000) was loaded to synthesized particles with various drug concentrations ($150, 300, 400, 500, 600\mu\text{g/ml}$) in potassium phosphate buffer (PBS) purchased from Sigma–Aldrich Co. Chemical structure representation of DOX is given in Figure 7.18.

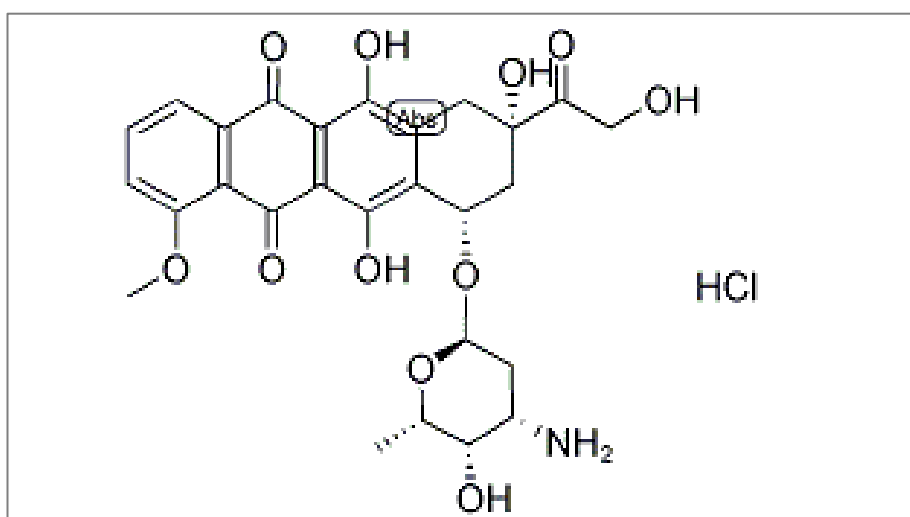


Figure 7.18: Chemical structure representation of DOX [80].

The mixture of Fe_2O_3 nanoparticles coated with the biopolymers (2.5 mg/ml), Doxorubicin and potassium phosphate buffer was rotated (MARKA Rotator) at 90 rpm with 5 s vibration intervals for 24 h in the light protected tubes at room temperature. Then, Doxorubicin loaded Fe_2O_3 nanoparticles coated with the

biopolymers were separated by magnetic decantation. The loading efficiency was quantified by measuring the absorbance values of unloaded drug in the supernatant with a UV-spectrophotometer at 481 nm [81].

Drug loading efficiency is obtained with uv/vis Spektrophotometer by using the formula below.

$$\text{Loading Efficiency(\%)} = \frac{(\text{total } \mu\text{g of drug added}) - (\mu\text{g of drug in supernatant})}{(\text{total } \mu\text{g of drug added})} \times 100 \quad (7.3)$$

The Figure 7.19 shows drug loading efficiencies of 1g/L HEC+2% Fe₂O₃, for 1g/L NC+2% Fe₂O₃ particles.

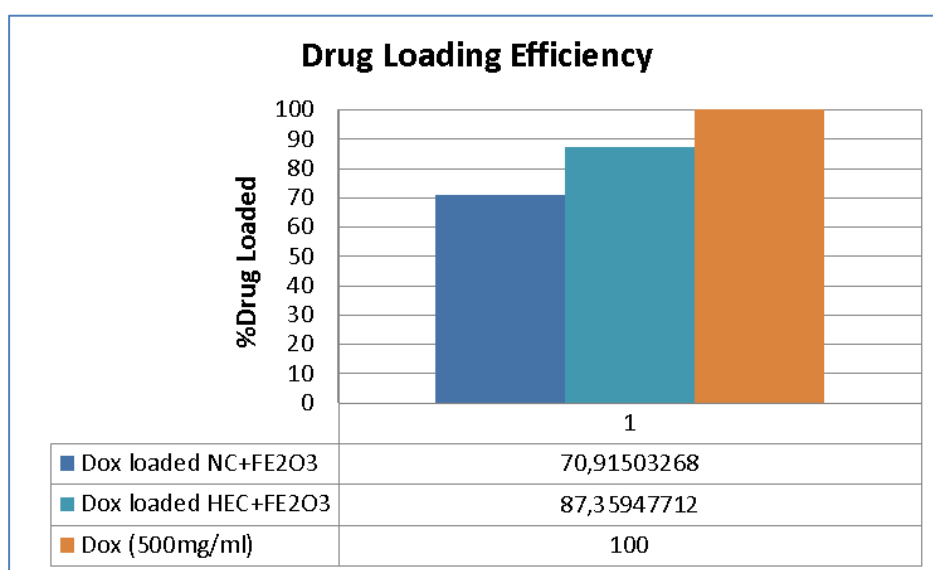


Figure 7.19: Drug loading % of 1g/L HEC+2% Fe₂O₃, for 1g/L NC+2% Fe₂O₃ particles.

7.7.4.1 In vitro evaluations for DOX loaded nanoparticles

Particles were loaded with DOX, which is an antitumor drug with methods mentioned at section 7.7.4. Loading efficiencies were calculated and drug loading capacities were obtained. Later DOX loaded particles were tested with MCF7 cell line to examine drug loading effects of nanoparticles and their effect on the viability of the cells. Cell viability % of MCF7 cells were determined the results are given in Figure 7.20.

The results show that DOX was successfully loaded to particles and had a drastic effect on the cell viabilities. Toxicity of the DOX loaded particles are very high at 400, 250, 200 µg/ml concentrations. DOX loaded 1g/L HEC+2% Fe₂O₃ particles

showed more toxicity than DOX loaded 1g/L NC+2% Fe_2O_3 particles, These results were as expected because 1g/L HEC+2% Fe_2O_3 particles were able to adsorb more DOX than NC polymer coated particles (as seen in Figure 7.19).

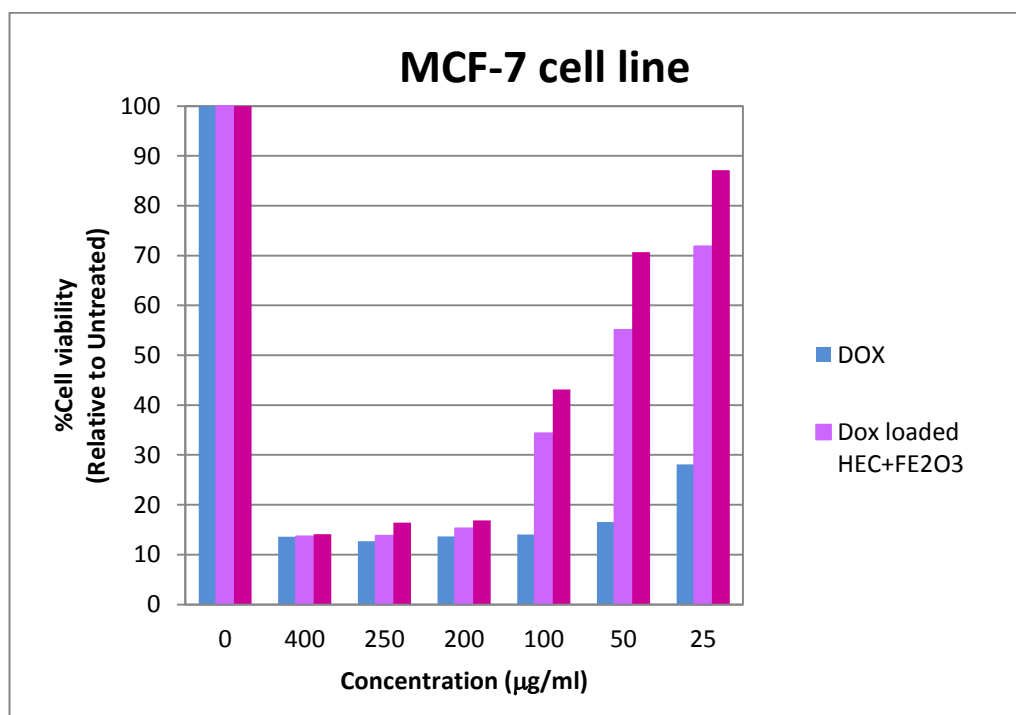


Figure 7.20: Relative cell viability (%) of MCF-7 treated with DOX loaded 1g/L HEC+2% Fe_2O_3 and 1g/L NC+2% Fe_2O_3 particles.

8. CONCLUSIONS

In this study the goal was to synthesize multifunctional magnetic nanoparticles with optimum properties suitable for using in targeted drug delivery systems. When designing and synthesizing multifunctional nanoparticles all advantages and disadvantages were considered. Chosen polymers for this study were HEC and NC which are cellulosic and biocompatible. To reach a positive result characterization of particles and optimum polymer concentration determination is important. Characterization techniques are required to determine magnetic nanoparticle properties such as size, crystal structure, material's thermal stability, absorption spectrum and magnetic behavior. The stable and fully covered surfaces of the MNPs were characterized by the conventional methods such as scanning electron microscopy (SEM) for the determination of the size and morphology, X-ray diffraction (XRD) to determine crystal structure, Fourier transform infrared spectroscopy (FTIR) to analyze the chemical bonds and functional groups, thermogravimetric analysis (TGA) to determine material's thermal properties and vibrating sample magnetometers (VSM) to measure the magnetic properties. After the characterization of MNP, the *in vitro* evaluations will give insight about biological compatibility and toxicity of synthesized particles.

Rheological and electrokinetic measurements provided significant information for determining the optimum biopolymer concentrations. The rheological and the electrokinetic measurements did not show much change in the flow or the aggregation behavior for the biopolymer HEC. On the other hand, Zeta potential measurements showed that HEC covered the whole surfaces of the iron oxide particles after the 0.05g/L HEC concentration. Because HEC did not change any structural properties of Fe_2O_3 nanoparticles it can be said that the attachment of HEC to the Fe_2O_3 particle surfaces is completely caused by electrosteric effects. Positively charged HEC were attracted to the negatively charged surface of Fe_2O_3 and HEC changed the charge distribution on the Fe_2O_3 surface, which reduced the entropy of

the particle. Rheological and the electrokinetical behaviours of NC biopolymer were very similar to HEC, only NC was not able to cover Fe_2O_3 surface as much as HEC.

Magnetorheometers are used for studying the changes in flow properties that occur in fluids which are exposed to controlled magnetic fields. When an external magnetic field is applied, there is a drastic change on the flow properties of the magnetic suspensions. Because only possibility to target MNPs to desited sites is to apply external magnetic field, assessment of magnetorheological flow properties are crutial for designing MNPs suitable for drug delivery systems. Magnetorheological results of synthesized MNPs showed similar results for both HEC and NC polymers. Resuts indicated that as polymer concentration increased viscosity of biopolymer coated Fe_2O_3 particles (under applied magnetic field) decreased. Espessially for 1g/L of polymer concentrations the desired magnerorheological properties were observed for both polymers HEC and NK. This property gained by adsorbing polymers to Fe_2O_3 surface can aid nanoparticles to have fluid behaviours instead of solid phase behaviours under applied magnetic field. This is an advantage for MNP drug delivery systems because when they are used in systematic applications MNPs should have fluid flow behavior under magnetic fields to reach the target site.

FTIR measurements showed that characteristic Fe-O streching vibration peak of Fe_2O_3 was at 576 cm^{-1} . The results indicated that addition of the polymers HEC and NC did not change the spectrum of Fe_2O_3 but characteristic Fe-O vibration peaks were slightly shifted. The reason for this shift was overlapping of polymer and Fe_2O_3 peaks. No binding peaks were observed as expected.

The crystal structure of Fe_2O_3 and Fe_2O_3 in the presence of HEC was measured by X-Ray diffraction analysis. According to the results, no changes were determined as HEC concentration changed. Therefore, crystal structure was not affected by polymer interactions.

Scanning electron microscopic (SEM) images of the samples were used for characterization of the dispersions with the polymer effect. Direct evidence of surface modification of the dispersion can be seen in SEM examination of the cross-section of particles (at section 7.5.6). SEM images of all Fe_2O_3 nanoparticles and HEC biopolymer coated Fe_2O_3 nanoparticles were obtained for particle size determination and imaging. HEC polymer appeared on the ironoxide particles as

dotted texture. The increasing concentration of HEC polymer increased the number of coated Fe₂O₃ nanoparticles as seen on the SEM pictures.

For the further studies, it is decided to use 1g/L HEC and 1g/L NC concentration for synthesizing multifunctional magnetic Fe₂O₃ nanoparticles because of the reasons above. After optimum concentrations of biopolymers were chosen, Thermo-gravimetric analyses *in vitro* toxicity evaluations were executed and magnetic properties of synthesized Fe₂O₃ nanoparticles were examined.

Because targeting of multifunctional magnetic Fe₂O₃ nanoparticles will be with magnetic field applications and manipulations it is important that particles do not lose their magnetic properties. Whether biopolymer coating of Fe₂O₃ nanoparticles affected their magnetic properties were examined with vibrating sample magnetometer. The results indicated that polymer adsorption to Fe₂O₃ particles reduced the magnetization values slightly but did not change the characteristic response of Fe₂O₃ particles to the magnetic field.

The thermal analyses of the samples were determined using thermo gravimetric (TG) and differential thermal analysis (DTA). The results showed uncoated Fe₂O₃ particles gained significant amount of weight at temperatures in the range of 30 to 300 °C. This indicates that these particles were oxidized when uncoated. Coated and uncoated Fe₂O₃ particles showed different weight lost events. HEC and NC coated particles were not oxidized because of coatings prevented Fe₂O₃ particles to interact with the environment, so, they are not oxidized and they lost weight due to the polymers weight lost.

We have mentioned that evaluating the toxicological effects of MNPs both *in vitro* is crucial for the development of multifunctional magnetic Fe₂O₃ nanoparticles for using in medical applications. In order to assess whether synthesized Fe₂O₃ nanoparticles could have anticancer drug potential and targeted drug delivery properties *in vitro* evaluations were performed. To examine the toxicity of synthesized Fe₂O₃ nanoparticles, cytotoxicity assays were performed for all nanoparticle samples using MTS assays. First, cytotoxicity assays were performed on healthy cells to examine the toxic effects of Fe₂O₃ particles and their biopolymer-coated samples. Cytotoxicity assays showed that HEC coated Fe₂O₃ nanoparticle dilutions has considerably less toxicity to osteoblast cells than uncoated Fe₂O₃

dilutions. Experimental values indicate that HEC coated Fe_2O_3 nanoparticles has less cell toxicity and these nanoparticles may have potential to be used as a drug targeting and delivering model with less toxicity to healthy cells like osteoblast cell lines.

After testing toxicity of biopolymer-coated nanoparticles on healthy cells, the particles were loaded with DOX, which is an antitumor drug. Loading efficiencies were calculated and drug loading capacities were obtained. As the results showed 1g/L HEC + 2% Fe_2O_3 and 1g/L NC + 2%, Fe_2O_3 particles were able to adsorb DOX at 87.36% and 70.92 % capacity (respectively).

Later DOX loaded particles were tested with MCF7 cell line to examine drug loading effects on nanoparticles and viability of cells. The results showed that DOX was successfully loaded to particles and toxicity of the DOX loaded particles were very high at 400, 250, 200 $\mu\text{g/ml}$ concentrations. DOX loaded 1g/L HEC+2% Fe_2O_3 particles showed more toxicity than DOX loaded 1g/L NC+2% Fe_2O_3 particles, These results were as expected because 1g/L HEC+2% Fe_2O_3 particles were able to adsorb more DOX than NC polymer coated particles.

In conclusion, this study showed that 1g/L HEC+2% Fe_2O_3 and 1g/L NC+2% Fe_2O_3 particles have the potential to be used in drug delivery systems for cancer therapies and also in hyperthermia treatments. For further studies, *in vivo* effects of these particles are planned to be examined to determine their systematic interactions within a living organism.

REFERENCES

- [1] **Winer, J. L., et al.** (2012). "The Use of Nanoparticles as Contrast Media in Neuroimaging: A Statement on Toxicity." *World Neurosurgery* 78(6): 709-711.
- [2] **Mahmoudi, M., et al.** (2010). "A new approach for the *in vitro* identification of the cytotoxicity of superparamagnetic iron oxide nanoparticles." *Colloids and Surfaces B: Biointerfaces* 75(1): 300-309.
- [3] **Rivera Gil, P., et al.** (2010). "Nanopharmacy: Inorganic nanoscale devices as vectors and active compounds." *Pharmacological Research* 62(2): 115-125.
- [4] **Chan, W. C. W., et al.** (2002). "Luminescent quantum dots for multiplexed biological detection and imaging." *Current Opinion in Biotechnology* 13(1): 40-46.
- [5] **Sonvico, F., et al.** (2005). "Metallic colloid nanotechnology, applications in diagnosis and therapeutics. " *Curr Pharm Des* 11(16): 2095-2105.
- [6] **Mahmoudi, M., et al.** (2011). "Superparamagnetic iron oxide nanoparticles (SPIONs): Development, surface modification and applications in chemotherapy", *Advanced Drug Delivery Reviews*, Vol.63, pp.24–46.
- [7] **Mahmoudi, M., et al** (2009). "An *in vitro* study of bare and poly(ethylene glycol)-co-fumarate coated superparamagnetic iron oxide nanoparticles: a new toxicity identification procedure", *Nanotechnology*, Vol.20, pp. 225104.
- [8] **Mahmoudi, M., Simchi, A., Milani, A.S., Stroeve, P.** (2009). "Cell toxicity of superparamagnetic iron oxide nanoparticles", *Journal of Colloid and Interface Science*, Vol.336, pp.510-518.
- [9] **Koehler, F. M., et al.** (2008) "Magnetic EDTA: Coupling heavy metal chelators to metal nanomagnets for rapid removal of cadmium, lead and copper from contaminated water", *Chem. Commun.*, 32: 4862–4865.
- [10] **Ayyappan, S., et al.** (2010). "Influence of Co²⁺ Ion Concentration on the Size, Magnetic Properties, and Purity of CoFe₂O₄ Spinel Ferrite Nanoparticles", *J. Phys. Chem.*, , 114: 6334–6341.
- [11] **Ahn, C. H., Choi, J. W., Cho, H. J.** (2004). *Encyclopedia of Nanoscience and Nanotechnology*, Nalwa H. S. (Ed.), Vol. 6, p. 815, American Scientific Publishers, Stevenson Ranch, CA.
- [12] **Jakubovics, J. P.** (1994). *Magnetism and magnetic materials*, Institute of Materials.
- [13] **Willard, M. A., et al.** (2004) *Encyclopedia of Nanoscience and Nanotechnology*, Nalwa H. S. (Ed.), Vol. 1, p. 815, American Scientific Publishers, Stevenson Ranch, CA.

- [14] **Leslie-Pelecky, D. L., Rieke, R. D.** (1996). "Magnetic Properties of Nanostructured Materials." *Chemistry of Materials* 8(8): 1770-1783.
- [15] **Laurent, S., et al.** (2008). "Magnetic Iron Oxide Nanoparticles: Synthesis, Stabilization, Vectorization, Physicochemical Characterizations, and Biological Applications." *Chemical Reviews* 108(6): 2064-2110.
- [16] **Griffiths, D. J.** (1999). *Introduction to electrodynamics*. Upper Saddle River, N.J: Prentice Hall.
- [17] **Dronskowski, R.** (2001). "The Little Maghemite Story: A Classic Functional Material." *Advanced Functional Materials* 11(1): 27-29.
- [18] **Cornell, R. M., Schwertmann, U.** (2004). *Introduction to the Iron Oxides*. The Iron Oxides, Wiley-VCH Verlag GmbH & Co. KGaA: 1-7.
- [19] **Krishnan, K. M.** (2010). "Biomedical Nanomagnetism: A Spin Through Possibilities in Imaging, Diagnostics, and Therapy. *IEEE Transactions on Magnetics*, 46(7), 2523–2558. doi:10.1109/TMAG.2010.2046907
- [20] **Jiles, D.** (1998). *Introduction to Magnetism and Magnetic Materials*, London, CRC Press.
- [21] **Coey, J.M.D.** (2009). *Magnetism and Magnetic Materials*. Cambridge University Press.
- [22] **Thanh, N.T.** (2011). *Magnetic Nanoparticles: From Fabrication to Medical and Clinical Applications*. CRC Press.
- [23] **Singh, D., McMillan, J. M., Liu, X.-M., Vishwasrao, H. M., Kabanov, A. V., Sokolsky-Papkov, M., & Gendelman, H. E.** (2014). Formulation design facilitates magnetic nanoparticle delivery to diseased cells and tissues. *Nanomedicine* (London, England), 9(3), 469–485. doi:10.2217/nnm.14.4
- [24] **Lee, J.-H., et al.** (2011). "Exchange-coupled magnetic nanoparticles for efficient heat induction." *Nat Nano* 6(7): 418-422.
- [25] **Shubayev, V. I., et al.** (2009). "Magnetic nanoparticles for theragnostics." *Advanced Drug Delivery Reviews* 61(6): 467-477.
- [26] **Wankhede, M., Bouras, A., Kaluzova, M., & Hadjipanayis, C. G.** (2012). "Magnetic nanoparticles: an emerging technology for malignant brain tumor imaging and therapy". *Expert Review of Clinical Pharmacology*, 5(2), 173–186. doi:10.1586/ecp.12.1
- [27] **Hildebrandt B., Wust P., Ahlers O., et al.** (2002). "The cellular and molecular basis of hyperthermia". *Crit. Rev. Oncol. Hematol.* 43(1), 33–56.
- [28] **Wust P., Hildebrandt B., Sreenivasa G., et al.** (2002). "Hyperthermia in combined treatment of cancer". *Lancet Oncol.* 3(8): 487–497.
- [29] **Johannsen M., Gneveckow U., Taymoorian K., et al.** (2007). "Morbidity and quality of life during thermotherapy using magnetic nanoparticles in locally recurrent prostate cancer: Results of a prospective phase I trial." *Int. J. Hyperth.* 23(3): 315–323.
- [30] **Maier-Hauff K., Rothe R., Scholz R., et al.** (2007). "Intracranial thermotherapy using magnetic nanoparticles combined with external

- beam radiotherapy: Results of a feasibility study on patients with glioblastoma multiforme." *J. Neurooncol.* 81(1): 53–60.
- [31] **Maier-Hauff K., Ulrich F., Nestler D., et al.** (2011). "Efficacy and safety of intratumoral thermotherapy using magnetic iron-oxide nanoparticles combined with external beam radiotherapy on patients with recurrent glioblastoma multiforme." *J. Neurooncol.* 103(2): 317–324.
- [32] **Matsumine A., Takegami K., Asanuma K., et al.** (2011). "A novel hyperthermia treatment for bone metastases using magnetic materials." *Int. J. Clin. Oncol.* 16(2): 101–108.
- [33] **Corchero, J. L., Villaverde, A.** (2009). "Biomedical applications of distally controlled magnetic nanoparticles." *Trends in Biotechnology* 27(8): 468-476
- [34] **Schwarz, J. A., et al.** (2004). *Dekker Encyclopedia of Nanoscience and Nanotechnology*, CRC Press, p. 865-880.
- [35] **Müller, R., Steinmetz, H., Hiergeist, R., Gawalek, W.** (2004) "Magnetic particles for medical applications by glass crystallization." *J. Magn. Magn. Mater.* 272-276:1539-1541. DOI: 10.1016/S0304-8853(03)01582-8
- [36] **Häfeli, U. O. and G. J. Pauer** (1999). "In vitro and in vivo toxicity of magnetic microspheres." *Journal of Magnetism and Magnetic Materials* 194(1–3): 76-82.
- [37] **Vadala, M. L., et al.** (2005). "Cobalt–silica magnetic nanoparticles with functional surfaces." *Journal of Magnetism and Magnetic Materials* 293(1): 162-170.
- [38] **Häfeli, U. O.** (2004). "Magnetically modulated therapeutic systems." *Int. J. Pharm.* 277: 19-24.
- [39] **Rosengart, A. J. et al.** (2005). "Magnetizable implants and functionalized magnetic carriers: A novel approach for noninvasive yet targeted drug delivery." *Journal of Magnetism and Magnetic Materials* 293(1): 633-638.
- [40] **Yellen, B. B. et al.** (2005). "Targeted drug delivery to magnetic implants for therapeutic applications." *Journal of Magnetism and Magnetic Materials* 293(1): 647-654.
- [41] **Jordan, A., Scholtz, R., Wust, P., Fähling, H., Felix R.** (1999). "Magnetic fluid hyperthermia (MFH): Cancer treatment with AC magnetic field induced excitation of biocompatible superparamagnetic nanoparticles." *J. Magn. Magn. Mater.* 201(1): 413-419.
- [42] **Brandenburg, U., Lagaly, G.** (1988). "Rheological properties of sodium-montmorillonite dispersions.", *Applied Clay Science*, **3**: 263-279.
- [43] **Watson, L. et al.** (2007). *Crude Oil Asphaltenes: Colloidal Aspects. Encyclopedia of Surface and Colloid Science*, Second Edition, Taylor & Francis. null: 1-18.
- [44] **Olphen, H.** (1979). *Data Handbook for Clay Materials and other non-Metallic Minerals*, Oxford Pergamon Press

- [45] **Neaman, A., Singer, A.** (2000). "Reology of Mixed Palygorskite-Montmorillonite Suspensions", *Clays and Clay Minerals*, 48: 713-715.
- [46] **Hunter, R.** (1987-1989). *Foundation of Colloid Science*, vol.1, Clarendon Press, Oxford.
- [47] **Hunter, R.** (1993). *Introduction to Modern Colloidal Science*, Oxford University Press, Oxford.
- [48] **Russel, W. B., Saville, D. A., Schowalter, W. R.** (1989). *Colloidal Dispersions*. Cambridge University Press: Cambridge.
- [49] **Liang, Y. et al.** (2007). "Interaction forces between colloidal particles in liquid: Theory and experiment." *Advances in Colloid and Interface Science* 134–135(0): 151-166
- [50] **Israelacvili, J.N.** (2011). *Intermolecular and Surface Forces*, Academic Press, 3rd ed. ISBN-13: 978-0123919274
- [51] **Liang, Y., et al.** (2007). "Interaction forces between colloidal particles in liquid: Theory and experiment." *Advances in Colloid and Interface Science* 134–135(0): 151-1662531396.
- [52] **Lagaly, G., Weiss, A.** (1969). "Determination of the layer charge in mica-type layer silicates" in L. Heller (ed.), *Proc. Int. Clay Conf.* Israel Univ. Press Jerusalem, 61-80.
- [53] **Khandal, R. K., Tadros, T. F.** (1988). "Application of viscoelastic measurements to the investigation of the swelling of sodium montmorillonite suspensions" , *Journal of Interfaces Science*, **125**: 122-128.
- [54] **Hiemenz, P. C., Rajagopalan, R.** (1997). *Principles of Colloid and Surface Chemistry*, Marcel Dekker, Newyork.
- [56] **Barnes, H.A., Hutton, J.F., Walters, K.** (1993). *An Introduction to Rheology* (2nd ed.) Elsevier Science publishers BV, Amsterdam.
- [57] **Neaman, A., Singer, A.** (2000). "Reology of Mixed Palygorskite-Montmorillonite Suspensions", *Clays and Clay Minerals*, **48**:713-715.
- [58] **Jobling, A.** (1991). "An introduction to rheology H. A. Barnes, J. F. Hutton and K. Walters, Elsevier Science Publishers, Amsterdam, 1989. pp. v + 199, Price \$6050/Dfl 115.00. ISBN 0-444-87469-0." *Polymer International* 25(1): 61-61.
- [59] **Hunter, R.J.** (1981). *Zeta Potential in Colloid Science*, Academic Press, New York
- [60] **Carlson, J. J., Kawatra, S. K.** (2013). "Factors Affecting Zeta Potential of Iron Oxides." *Mineral Processing and Extractive Metallurgy Review* 34(5): 269-303.
- [61] **Van Olphen, H.,** (1977). *Introduction to Clay Chemistry*, Willey, New York.
- [62] **Carlson, J.D., D. M. C., St. Clair, K. A.** (1997). Commercial magneto-rheological devices. 5 th International Conference on ER fluids, MR suspensions and associated technology, Sheffield, World Scientific

- [63] **Inoue, A. et al.** (1999). "Properties of ER Fluids Comprised of Liquid Crystalline Polymers." *International Journal of Modern Physics B* 13(14n16): 1966-1974
- [64] **Orihara, H., Doi, M. and Ishibashi, Y.** (1999). "Two types of mechanism of electrorheological effect in polymer blends", *International Journal of Modern Physics B* 13(14n16): 1949-1955.
- [65] **Domínguez-Delgado, C. L., et al.** (2014). *Drug Carrier Systems Using Chitosan for Non Parenteral Routes, Pharmacology and Therapeutics*, Dr. Sivakumar Gowder (Ed.), ISBN: 978-953-51-1620-2, InTech, DOI:10.5772/57235.
- [66] **Aspler, J. et al.,** (2013). *Review of Nanocellulosic Products and Their Applications, in Biopolymer Nanocomposites: Processing, Properties, and Applications* (eds A. Dufresne, S. Thomas and L. A. Pothen), John Wiley & Sons, Inc., Hoboken, NJ, USA. doi: 10.1002/9781118609958.ch20
- [67] **Verbeek., C. J. R.** (2012). *Products and Applications of Biopolymers*. Croatia, InTech. ISBN 978-953-51-0226-7
- [68] **Khalil, H. P. S. A., Bhat, A. H., & Yusra, A. F. I.** (2012). "Green composites from sustainable cellulose nanofibrils: A review." *Carbohydrate Polymers*, 87(2): 963–979
- [69] **Akil, H. M., et al.,** (2011). "Kenaf fiber reinforced composites: A review". *Materials and Design*, 32(8–9):4107–4121.
- [70] **Thakur, V. K., Thakur, M. K.** (2014). "Processing and characterization of natural cellulose fibers/thermoset polymer composites." *Carbohydrate Polymers* 109(0): 102-117.
- [71] **Lu, Y., Kim, S., & Park, K.** (2011). "In vitro-In vivo Correlation: Perspectives on Model Development." *International Journal of Pharmaceutics*, 418(1): 142–148. doi:10.1016/j.ijpharm.2011.01.010
- [72] **Goldstein, J., et al.** (2012). *Scanning Electron Microscopy and X-ray Microanalysis*, Third Edition, Springer US.
- [73] **Klug, H., Alexander, L.** (1996). *X-ray diffraction procedures*. 2 ed.; J. Wiley & Sons Inc.: New York,
- [74] **Cullity, B. D. and Stock, S. R.** (2001). *Elements of X-ray Diffraction*, Prentice Hall.
- [75] **Davis, S. P., et al.** (2001). *Fourier Transform Spectrometry*, Academic Press.
- [76] **Brown, M.E.** (2004). *Introduction to Thermal Analysis, Techniques and Applications*, Kluwer Academic Publishers.
- [77] **Alwa, H. S.** (2002). *Handbook of thin film materials*. Handbook of Thin Films. H. S. Nalwa. Burlington, Academic Press: xxiii-xxvi.
- [78] **2-Hydroxyethyl cellulose.** (2015). Retrieved from <http://www.sigmaaldrich.com/catalog/product/aldrich/434973?lang=en®ion=TR>, date retrieved 12.05.2015.
- [79] **Ives, K. J.** (2012). *The Scientific Basis of Flocculation*, Springer, Netherlands.

- [80] **Doxorubicin hydrochloride** (2015). Retrieved from <http://www.sigmaaldrich.com/catalog/product/sigma/d1515?lang=en®ion=TR>, date retrieved 12.05.2015.
- [81] **Wavelength Index**. (2015). Retrieved from <http://www.sigmaaldrich.com/life-science/cell-biology/detection/learning-center/wavelength-index.html>, date retrieved 12.05.2015.

CURRICULUM VITAE

Name Surname: Maide Gökçe BEKAROĞLU

Place and Date of Birth: Üsküdar, 30.03.1988

E-Mail: gbekaroglu@live.com

EDUCATION:

B.Sc.: Physics Engineer

PROFESSIONAL EXPERIENCE AND REWARDS:

RESEARCH EXPERIENCE :

Feb 2015–present , project assistant –TUBITAK (Project Title : Preparation of multifunctional magnetic nanoparticles for cancer therapy)

Sep 2013–Mar 2014 project assistant- TUBITAK (Project No: 113S251).

OTHER PUBLICATIONS, PRESENTATIONS AND PATENTS :

Bekaroğlu M.G., Arslan B.A. (2014) Natural Killer (NK) Cells in β Thalassemia Major Patients. JSM Biotechnol Bioeng 2(2): 1040

Atasever-Arslan, B., et al. (2015). "Cytotoxic effect of extract from *Dunaliella salina* against SH-SY5Y neuroblastoma cells." Gen Physiol Biophys.